이학박사학위논문

Study of highly sensitive and reproducible paper-based SERS sensors for detection of trace pesticides

미량의 농약 검출을 위한 고감도 고재현성의 종이 기반 표면 증강 라만 산란 센서 연구

2018년 2월

서울대학교 대학원

과학교육과 화학전공

이 민 우

Study of highly sensitive and reproducible paper-based SERS sensors for detection of trace pesticides

미량의 농약 검출을 위한 고감도 고재현성의 종이 기반 표면 증강 라만 산란 센서 연구

지도 교수 정 대 홍

이 논문을 이학박사학위논문으로 제출함
2018년 2월
서울대학교 대학원
과학교육과 화학전공
이 민 우

이민우의 이학박사학위논문을 인준함
2017년 11월

위 원 장 _____ (인)

부위원장 _____ (인)

위 원 _____ (인)

위 원 _____ (인)

위 원 _____ (인)

ABSTRACT

Study of highly sensitive and reproducible paper-based SERS sensors for detection of trace pesticides

Minwoo Lee

Department of Chemistry Education

The Graduate School

Seoul National University

As a cost-effective approach for detecting trace amounts of pesticides, paper-based surface-enhanced Raman scattering (SERS) sensors have been the subject of intensive research. However, one of the hurdles to overcome is the difficulty of retaining nanoparticles on the paper surface due to the hydrophilic nature of the cellulose fibers in paper. Furthermore, another hurdle is high surface roughness and non-uniformity of the paper surface due to the size variation and conformation of cellulose fibrils in paper. These hurdles reduce the sensitivity and reproducibility of paper-based SERS sensors due to the low density of nanoparticles, short retention time of analytes and non-uniform surface by many pores and high surface roughness on the paper surface. Furthermore, conventional SERS sensors have difficulty to use as universal SERS sensors due to difference of binding affinities between molecules and metal nanoparticle depending on functional groups of molecules.

In this study, a highly sensitive and reproducible filter paper-based SERS sensor was developed. To increase the sensitivity and reproducibility of the sensor, the hydrophilic nature of the filter paper was modified to become hydrophobic one by using alkyl ketene dimer (AKD) treatment. In addition, cellulose nanofibril (CNF) coating was applied to the hydrophobic filter paper to increase the uniformity of the paper surface by filling pores and reducing the surface roughness of the filter paper. Finally, using CNF coated hydrophobic filter paper, a charge-selective paper-based SERS sensor was developed to detect polar organic pollutants for expanding the generality of SERS based molecular detection.

Thus, this thesis contains three chapters that focus on: fabricating a highly sensitive and reproducible filter paper-based SERS sensor by hydrophobic modification, developing a uniform surface for the filter paper-based SERS sensor for highly reproducible SERS detection by introducing CNF coating, and applying the developed paper-based SERS sensor for fabricating of a charge-selective SERS detection to expand the generality of SERS based molecular detection.

Chapter I describes the fabrication of hydrophobically modified filter paper to increase sensitivity and reproducibility of paper-based SERS sensor. Conventional paper-based SERS sensors quickly absorb nanoparticle and analyte solutions because of their hydrophilic nature. In addition, the short retention time of the analyte solution on the paper surface provides insufficient time for the analyte to bond on the surface of the nanoparticle. Thus, conventional paper-based SERS sensors show low sensitivities and reproducibilities. To overcome disadvantages of conventional

paper-based SERS sensor, the surface of filter paper was modified hydrophobically by introducing AKD on filter paper. By introducing AKD on filter paper, the retention time of the silver nanoparticle (AgNP) and analyte solutions on the paper surface was increased because the AKD treatment changed hydrophilic nature of filter paper to hydrophobic one. The AKD treatment increased the contact angle of the aqueous AgNP solution, which consequently increased the density of AgNP on the paper-based SERS sensor within reduced contact area. In addition, the retention time of the aqueous solution was increased by preventing its rapid absorption into the filter paper, and the AgNP solution was dried on the paper surface without absoprtion to the filter paper. As a result, because the increased density of AgNP on a small contact area on hydrophobic filter paper, the number of increased SERS hot-spots, and strongly enhanced the SERS signal. The sensitivity and reproducibility of the SERS signal were optimized by controlling the distribution of AgNP on the surface of the filter paper, which was achieved by adjusting the concentration of the AgNP solution. The spot-to-spot variation of the SERS intensities of 4-aminothiophenol (4-ATP) at 25 AgNP spots on hydrophobic filter paper-based SERS sensor was approximately 6.2% of relative standard deviation (RSD), and the limits of detections (LODs) of thiram and ferbam were 0.461 and 0.491 nM, respectively. These proof-of-concept results indicate that this low-cost and easily fabricated paper-based SERS sensor can provide highly sensitive pesticide detection.

Chapter II describes reducing the surface roughness and pores of the filter paper-based SERS sensor using CNF coating for highly reproducible SERS detection.

Because of non-uniform filter paper surface originated from the large number of pores and high surface roughness, conventional paper-based SERS were difficult to measure uniform SERS signals, resulting in low reproducibility. To overcome the low reproducibility of paper-based SERS sensors, CNF coating was introduced on the surface of filter paper to fill the pores and to flatten the surface of filter paper. Double CNF coatings on the surface of the hydrophobic filter paper increased the coverage of AgNP on the paper surface from 87 to 95%. Furthermore, the AgNP were uniformly introduced onto the surface of the filter paper by reduced surface roughness and the number of pores on the paper surface were redcued, as confirmed using field-emission scanning electron microscopy (FE-SEM). Applying double CNF coatings on hydrophobic filter paper-based SERS sensor reduced the RSD of the SERS intensity from 28 to 9% and the LOD of 4-ATP from 3.782 to 0.426 nM. These CNF surface modifications on paper-based SERS sensor provided a base to fabricate a highly reproducible paper-based SERS sensor.

Chapter III describes the development of a paper-based SERS sensor for detecting polar organic pollutants to expand the generality of SERS based molecular detection. Conventional paper-based SERS sensors are difficult to use as universal SERS sensors because the functional group in molecule have different affinity toward the metal. To expand the generality of paper-based SERS sensor, a charge-selective paper-based SERS sensor was developed by modifying the surface charge of AgNP. The citrate ion capped AgNP were exhibited negative surface charge due to negative charged citrate ion and attracted positively charged molecule by electrostatic

attraction. However, it was hard to detect negatively charged molecule by electrostatic repulsion. To detect negatively charged molecules, the positively surface charged AgNP was fabricated by modifying the surface charge of AgNP by applying poly(diallyldimethylammonium chloride) (PDDA) on AgNP surface. The PDDA encapsulated AgNP (AgNP@PDDA) exhibited positive surface charge, and attracted negatively charged molecule. The introduction of PDDA on AgNP was confirmed by zeta-potential change and high resolution transmission electron microscopy (HR-TEM) images. Charged Raman dyes were applied to the charge-selective paper-based SERS sensor to verify its feasibility. By using charge-selective paper-based SERS sensor, positively charged Raman dyes were successfully detected using the AgNP spots, and negatively charged Raman dyes were successfully detected using the PDDA encapsulated AgNP (AgNP@PDDA) spots by electrostatic attraction.. To expand its applicability for field test, polar organic pollutants (e.g., aniline and benzoic acid derivatives) were detected using the charge-selective paper-based SERS sensor. Aniline and benzoic acid derivatives were detected by AgNP and AgNP@PDDA spots, respectively. Furthermore, aniline and benzoic acid were detected at low concentration of tens of micromolar concentration with a less than 10% RSDs. Thus, the developed charge-selective paper-based SERS sensor could expand the generality of SERS based molecular detection with a high sensitivity and reproducibility by modifying the surface charge of the AgNP.

Keywords: surface-enhanced Raman scattering (SERS), alkyl ketene dimer

(AKD), filter paper, paper-based SERS sensor, hydrophobic modification, sensitivity, reproducibility, cellulose nanofibrils (CNF), charge-selective SERS detection.

Student number: 2012-30411

TABLE OF CONTENTS

LIST OF TABLES

LIST OF FIGURES

LIST OF ABBREVIATIONS

4-ATP	4-aminothiophenol
4-MA	4-methylaniline
4-MB	4-methylbenzoic acid
AgNP	Silver nanoparticle
AgNP@PDDA	PDDA encapsulated AgNP
AKD	Alkyl ketene dimer
AN	Aniline
AuNP	Gold nanoparticle
AuNR	Gold nanorod
BA	Benzoic acid
CMC	Carboxymethyl cellulose
CNF	Cellulose nanofibrils
CNF	Cellulose nanofibril
DDA	Discrete dipole approximation
DW	Distilled water
E-beam	Electron-beam
E-field	Electric field
EM	Electromagnetic field
FE-SEM	Field-emission scanning electron microscope
HR-TEM	High resolution transmission electron microscope
LOD	Limit of detection
LSPR	Localized surface plasmon resonance
MO	Methyl orange
NA	Numerical aperture

P4VP	Poly(4-vinylpyridine)
PDA	Polydophamine
PDDA	Poly(diallydimethylammonium chloride)
PDMS	Polydimethylsiloxane
PPS	Parker Print Surf
PVP	Polyvinylpyrrolidone
R6G	Rhodamine 6G
RSD	Relative standard deviation
$Ru(bpy)_3$	Tris(2,2'-bipyridyl)ruthenium(II) Chloride Hexahydrate
SAM	Self-aseembled monolayer
SEM	Scanning electron microscope
SERS	Surface-enhanced Raman scattering
SY	Sunset yellow
TEM	Transmission electron microscopy
UV/Vis	Ultraviolet/visible

Study of highly sensitive and reproducible paper-based SERS sensors for detection of trace pesticides

Introduction

1. History of surface-enhanced Raman spectroscopy (SERS)

Raman spectroscopy is a technique for identifying vibrational and rotational normal modes of molecule, and was discovered by C. V. Raman in 1928[1]. After its discovery, Raman spectroscopy became an attractive analytical technique because of several advantages: the technique is non-destructive and allows for non-contact measurement, the unique spectrum is produced by structure of molecule, and sample preparation is simple[2]. However, because of the small Raman cross section, Raman scattering shows weak signal, resulted in poor sensitivity. Thus, in the early stage, Raman spectroscopy was only used for limited applications[3]. However, in 1974, Fleischmann et al. discovered that Raman scattering of pyridine was significantly enhanced by its absorption on a silver electrode. This phenomena was called as surface-enhanced Raman scattering (SERS)[4]. The mechanisms of SERS enhancement originate from electromagnetic (EM) enhancement and chemical enhancement[5]. The exact mechanism is still under debate, however EM enhancement is a more dominant mechanism for SERS enhancement known by several studies[5-6]. The EM enhancement occurs when a molecule is placed near a metallic nanostructure, and the Raman scattering of molecule is enhanced by the localized surface plasmon resonance (LSPR) of the metallic nanostructure[7-8].

The discovery of the SERS phenomenon overcame the poor sensitivity of Raman spectroscopy. Furthermore, the SERS phenomenon is suitable for multiplexed

detection because of the intrinsic SERS signal of each molecule and the narrow bandwidth of the Raman spectrum[9]. Since its discovery, SERS has been used for a variety of applications, such as biosensor[10-12], food detection[13-14], chemical detection[15-16], and in the fields of art[17], life science[18-20], environmental science[21-23], electrochemistry[24-25].

Despite the advantages of SERS, even the same SERS sensors, the SERS signals of sensors were shown poor reproducibility because the state of the metallic nanostructure, such as its shape, size, conformation, and kinds of metal atoms, affected the SERS signal[7]. Especially, the SERS signal is more enhanced when a molecule lies on the edge or at a gap in the metallic nanostructure by concentration of local EM field of nanostructure[26-27], and this region is referred to as a SERS hot-spot[28]. By the reason, although the SERS sensors are fabricated with same methods, SERS sensors can exhibit different SERS intensities, and they cause several issues, such as reproducibility and reliability for molecular detection[29-31]. Furthermore, the lack of a universally applicable substrate for molecular detection is a disadvantage of SERS[32-34]. The SERS signal of a molecule is affected by the distance between the molecule and the metal, and the SERS signal dramatically decreases as the molecule moves away from the surface of the metallic nanostructure[35]. However, because of the affinity difference between molecule and metal[34], molecules with high affinities toward the metal, such as thiol (-SH)[32] and isocyanide (-NC)[36], produced

significantly enhanced SERS signals, however molecules with low affinities toward the metal are hard to detect using SERS because the molecules are not close enough to the surface of the metallic nanostructure. Therefore, it is difficult to produce universal SERS-based molecular detection sensors, and many researchers have tried to develop SERS sensors using various methods and substrates to overcome the disadvantages of SERS.

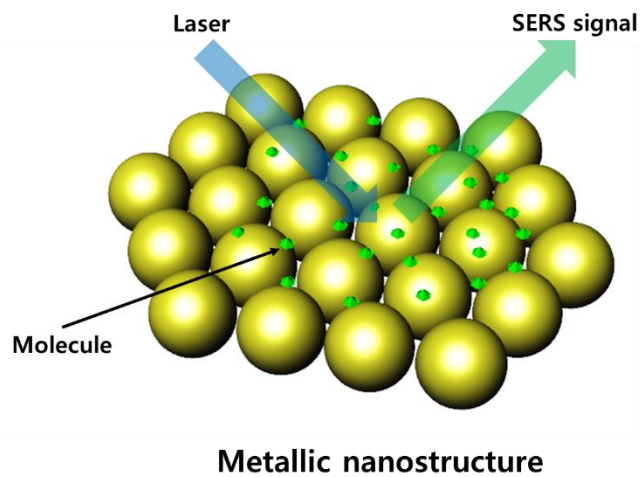

Figure 1. Conceptional illustration of SERS.

2. Development of SERS sensors

Ideal SERS sensors should satisfy the following requirements: 1) easy and cheap fabrication, 2) highly sensitive detection, 3) reliable and reproducible detection, 4) universal molecule detection, and 5) quantitative detection[33, 37-38]. To increase sensitivity and reproducibility of SERS sensors, SERS sensors have been developed using various methods and substrates. In the early stage of development, SERS sensors were fabricated as metal film on solid supports[39-41]. Metal film on solid support was deposited by vacuum sputtering or evaporating metal atom onto solid supports. Vacuum deposition produced metal films with numerous nano-sized cracks on solid supports, resulting in an enhanced SERS signal. However, the cracks were randomly distributed in the metal film, resulted in poor reproducibility and reliability. To increase the reproducibility of SERS sensors, wet etching[42-44] and lithography[45-53] based SERS sensors arose as attractive fabrication methods. Wet etching based SERS sensors used liquid-phase etchants, such as HF[44], KOH[42] and tetramethylammonium hydroxide to etch the solid supports[54], such as such as silicon[42-43] and aluminum[44] to fabricate periodic patterns on solid supports followed by metal deposition for fabrication SERS sensors. Chao et al. developed various surface morphologies on silicon wafer by optimizing the etching conditions to fabricate SERS sensor[42]. Furthrmore, Mehrvar et al. developed double nanocone array by applying wet etching on silicon wafer to fabricate SERS sensor[43]. However,

wet etching based SERS sensor was shown several disadvantages such as toxicity issue and substrate contamination by etchants, and inappropriate for fine adjustment of metallic nanostructures to optimization of SERS signal. The lithography method was introduced to fabricate the SERS sensor in a different way from wet etching, lithography based SERS sensors are fabricated the SERS sensors using two different methods, which are electron-beam (E-beam) lithography and nanosphere lithography. E-beam lithography is a method to fabricate custom shape on solid support covered by an electron-sensitive film called a photo-resist. Kahl et al. developed periodically structured metallic substrates on silicon wafer using E-beam lithography[47]. After that, various nanostructure shapes, such as squares, disks, triangles, and ellipse dimers, were developed as SERS sensors using E-beam lithography[45, 48-49]. Another type of lithography is nanosphere lithography, which fabricates 2D periodic nanostructure arrays by metal deposition on a solid support using polystyrene or SiO_2 bead arrays[50-53]. After metal deposition, polystyrene and SiO_2 bead arrays were removed using etchants. Lithography-based SERS sensors are suitable for mass-produce, fabricating highly uniform surface and reproducible SERS signals. In addition, they fabricate the SERS sensors in elaborate, custom shapes to optimize SERS detection[51, 53]. However, lithography-based techniques show the disadvantages inpoint of toxicity issue during the fabrication process and highly expensive price because of complex process and expensive instrumentation.

Many researchers have developed SERS sensors using nanoparticle instead of metal deposition on solid supports as a another approach to fabricate SERS sensors. To bind nanoparticle on solid support, Natan et al, fabricated a self-assembled monolayer (SAM) of a metal colloid on transmission electron microscopy (TEM) grid to create SERS sensor[55]. To introduce a SAM of nanoparticles on the solid support, the surface of the solid support (e.g., glass or silicon wafer) was modified using molecule with functional group, such as amine and thiol[56-57]. Furthermore, using bifunctional molecules, which have dithiol or diamine functional group, the 3D structure of multi-layered nanoparticles was developed by introducing a chemical linker between the SAM of the nanoparticles. SERS sensors with 3D structure of nanopartilces were reported to enhance the SERS signal more than 2-3 orders of magnitude[56, 58]. Polymers, such as polyvinylpyrrolidone (PVP) and poly(4-vinylpyrrolidone) (P4VP) were also introduced onto a solid support to fabricate a SAM of nanoparticles by electrostatic attraction[59]. Yoon et al. recently fabricated AgNP dimers using P4VP-coated glass as universal SERS sensors[60]. Light-induced growth of nanoparticles on solid supports were also applied to develop SERS sensors[61-63].

These SERS sensors are fabricated using solid supports, such as glass[64-65], silicon wafers[66], and polydimethylsiloxane (PDMS)[67]. These substrates are suitable for producing SERS sensors that exhibit high sensitivities and reproducibilities.

However, the overall processes for fabricating SERS sensors using these substrates are complex and sophisticated, in some cases, expensive and complex equipment is often required to fabricate SERS sensors based on these substrates. Furthermore, solid supports are difficult to functionalize, not eco-friendly, and expensive. For these reasons, developing cheap, simple, and easily producible SERS sensors is required.

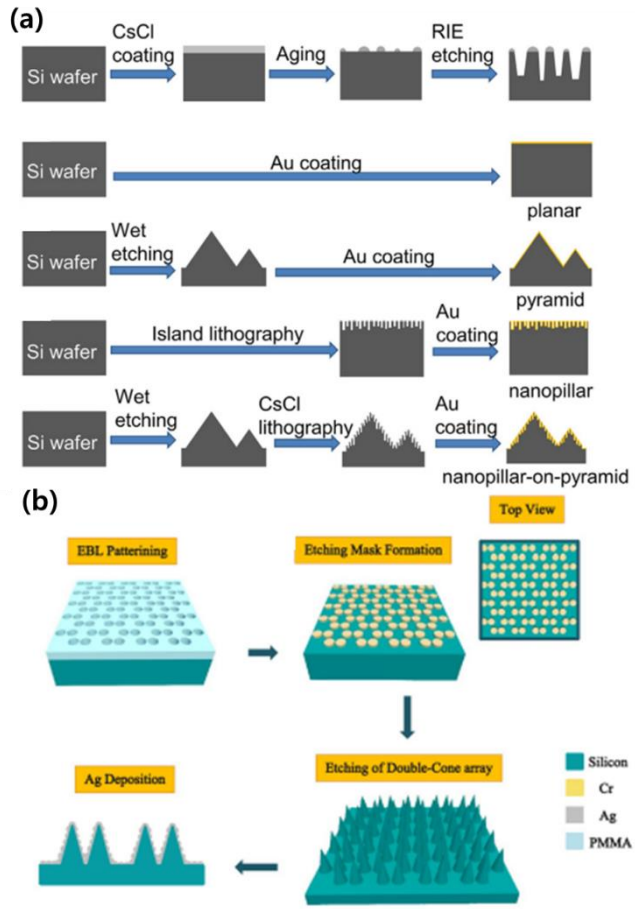

Figure 2. SERS sensors fabricated by wet etching. (a) Fabrication of various nanostructure using wet etching with different etching conditions[42], and (b) fabrication double nanocone array on silicon wafer[43].

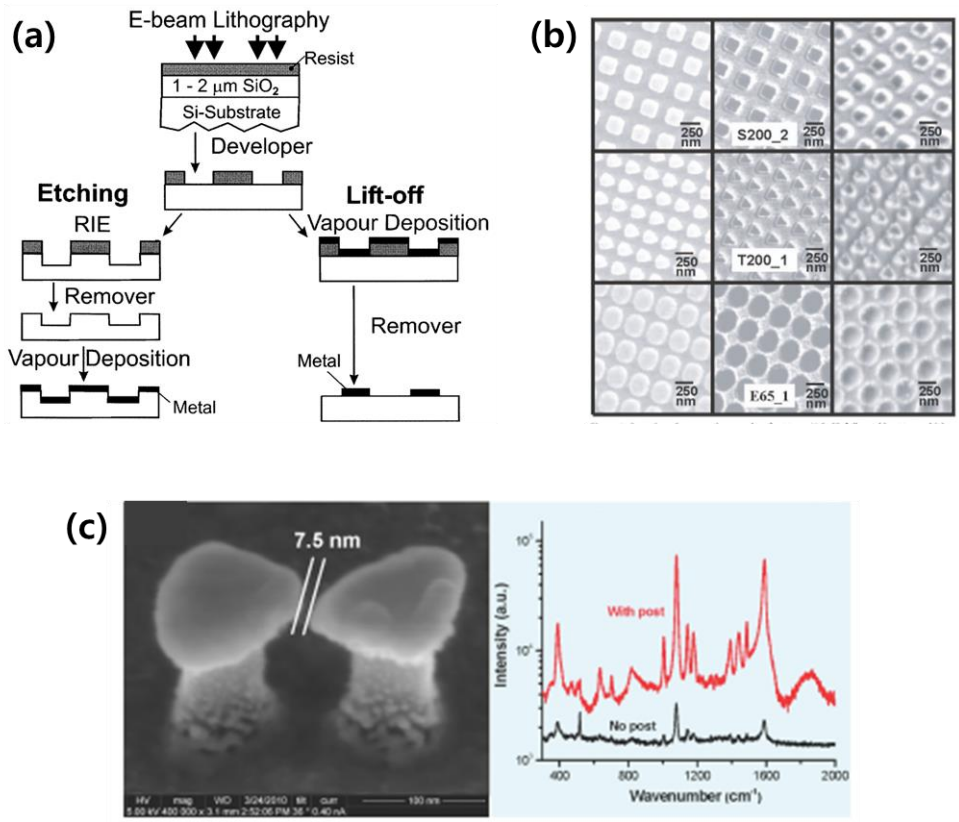

Figure 3. SERS sensors fabricated by lithography methods. (a) Scheme of fabrication of E-beam lithography based SERS sensor[47]. (b) Scanning electron microscope (SEM) image of various nanostructures fabricated by E-beam lithography[49], and (c) characterization of elevated gold bowtie on Si post. SEM image (left) and SERS spectra (right) of p-mercaptoaniline on elevated (red line) and non-elevated (black line) bowtie arrays on SERS sensor[46].

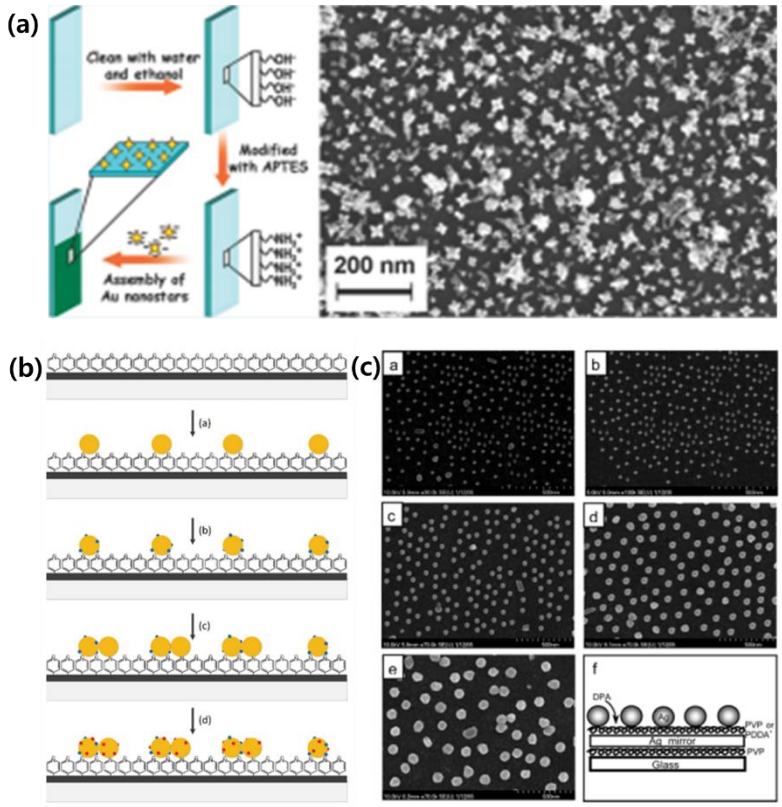

Figure 4. SERS sensors fabricated by SAM of nanoparticles. (a) Schematic illustration and field-emission scanning electron microscopy (FE-SEM) image of self-assembled gold nanostars[65]. (b) AgNP immobilization on the P4VP coated glass substrate. Blue dot means aniline, and red dot means target molecules[60], and (c) nanoparticle on film structure on PVP coated glass substrates, and SERS spectra of several molecules using SERS sensor[59].

3. Paper-based SERS sensors

Paper-based SERS sensors were developed as alternatives for overcoming the disadvantages of conventional SERS sensors. Paper-based SERS sensors show several advantages, including high flexibility, low cost, easy fabrication and functionalization of the paper surface, and good biodegradability and disposability[68]. Therefore, paper-based SERS sensors are emerging as potential replacements for the conventional SERS sensors.

In their early stage, paper-based SERS sensors were developed by direct nanoparticle growth on the paper surface[69-70]. Arthur et al. grew nanoparticle using Tollen's reaction on the filter paper surface[70], and Cabalín et al. grew nanoparticle by spraying reducing agents on wet filter paper treated with sliver nitrate solution[69]. After that, various methods, such as electrostatic adsorption[71-72], filtration[73], chemical- or light-induced deposition of nanoparticle[74-76], metal vapor deposition using metal evaporation[77], and screen and inkjet printing [78-79], have been studied to develop paper-based SERS sensors. In addition, paper-based SERS sensors have been applied to label-free detection of biological samples (e.g., cancer screening[80], on-site bioassay[81] and seminal plasma[82]), micro-fluidic channels for multiplexed detection[83], and lateral flow for biomolecule detection[84-85].

However, the aforementioned sensor fabrication methods still face drawbacks of non-uniform nanoparticle distribution, large spot-to-spot variation of the SERS

intensity, and requirement of complicated instrument, complex processes, and high substrate fabrication costs. Furthermore, it is difficult to retain the nanoparticles and analyte solution on the paper surface because of the hydrophilic nature of the paper, and the solution is quickly absorbed into the paper and become widely dispersed. The hydrophilic nature of the paper provides a low sensitivity and reproducibility because it is difficult to concentrate the analyte solution. In addition, because of the size variation and conformation of cellulose fibers in the paper, paper-based SERS sensors show high surface roughness and numerous pores, resulted in low reproducibility of the SERS signal. The affinity difference between the nanoparticle and molecule depending on functional group of molecule still affects the generality of the SERS sensor, and conventional paper-based SERS sensors was possible to detect only a few molecules which have specific functional group such as thiol, amine and isocyanide. This disadvantage hinders the expansion of generality of SERS based moelcular detection.

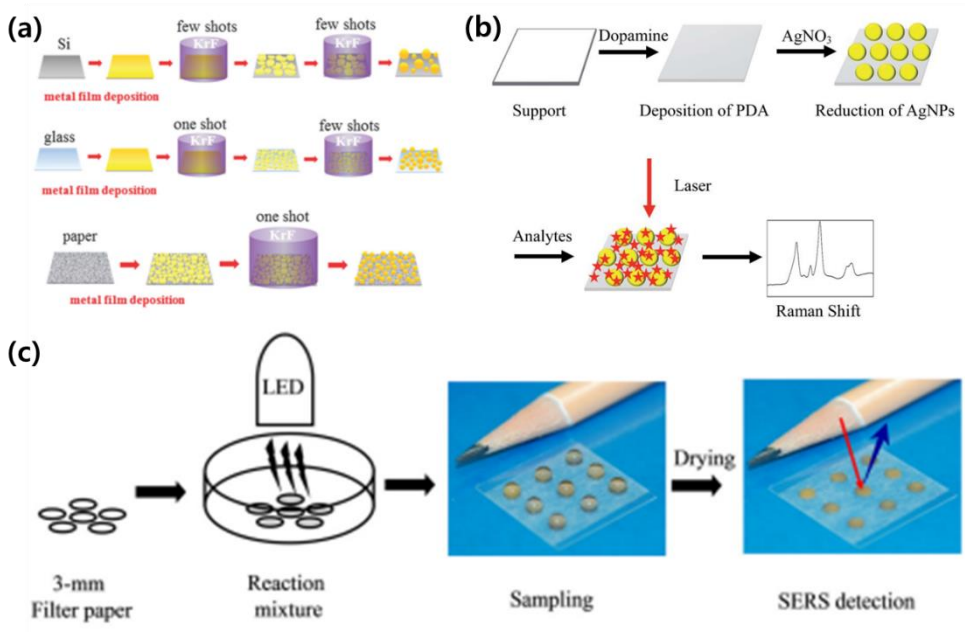

Figure 5. Paper-based SERS sensors by growth of nanoparticle on paper surface. (a) Schematic illustration of fabrication of nanoparticle on silicon wafer, glass and paper by laser-induced photothermal effect[77]. (b) Schmatic illustration of the growth of silver nanoparticle on polydophamine treated filter paper[86], and (c) fabrication of nanoparticles array on filter paper by irradiating LED[74].

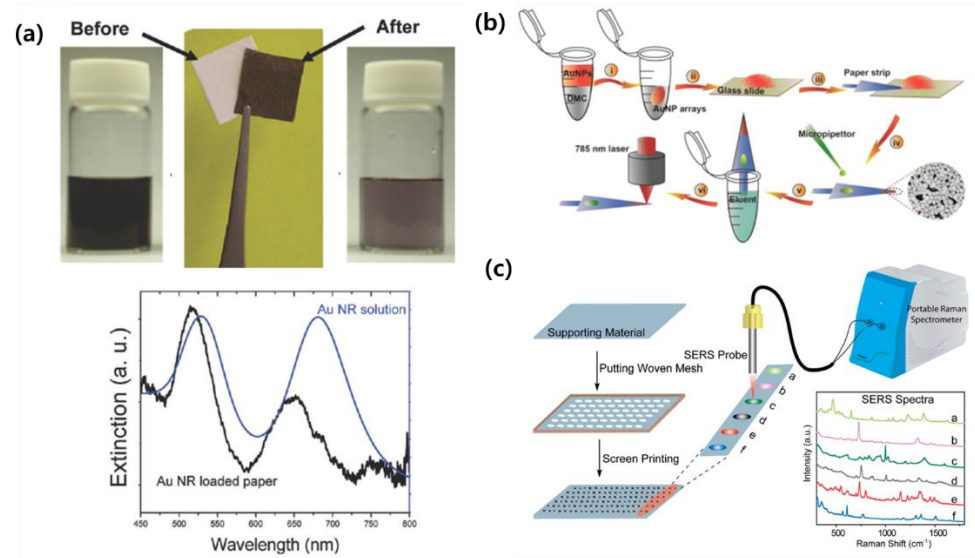

Figure 6. Paper-based SERS sensors by attachment of nanoparticles on paper surface. (a) Photographs and ultraviolet/visible (UV/Vis) extinction spectrum of gold nanorod coated filter paper[72]. (b) Schematic illustration of gold nanoparticle array loaded filter paper[87], and (c) schematic illustration of fabrication screen printed paper-based SERS sensor[78].

4. Research Objectives

In this study, a simple, inexpensive, and easily fabricated filter paper-based SERS sensor with high sensitivity, reproducibility, and expanding generality of SERS based molecular detection was designed and fabricated by modifying the surface of the filter paper and nanoparticle to overcome the disadvantages of conventional paper-based SERS sensors.

At first, hydrophobic modification of filter paper was described to increase sensitivity and reproducibility of paper-based SERS sensor in chapter I. Due to the hydrophilic property of paper-based SERS sensor, the aqueous solutions of nanoparticle and analyte were quickly absorbed and spread into the paper. As a result, the paper-based SERS sensor showed low sensitivity and reproducibility. To overcome disadvantage of conventional paper-based SERS sensor, hydrophillic property of filter paper was changed hydrophobic one by treatment of AKD on filter paper.

Secondly, fabrication of a uniform and smooth paper-based SERS sensor is described in chapter II. To increase the sensitivity of the paper-based SERS sensors, the SERS spectra were measured using a objective lens with high numerical aperture (NA) to increase the solid angle of the scattered light. However, using a objective lens with high NA for SERS measurement, conventional paper-based SERS sensors showed a low reproducibility because of their high surface roughness and numerous pores on

the paper surface. To fabricate a highly uniform and smooth paper-based SERS sensor, cellulose nanofibrils (CNFs) were introduced on the surface of the hydrophobically modified filter paper. By CNF coating, the surface roughness and the number of pores reduced, and the uniformity of filter paper was increased, resulted in increasing reproducibility of paper-based SERS sensor.

Finally, fabrication of a charge-selective paper-based SERS sensor to detect polar organic pollutants is described in chapter III. Because of the different affinity between the molecule and metal, only a few molecules could be detected by conventional SERS sensors. Thus, in order to expand the generality of SERS based molecular detection, polar organic pollutants, which was hard to detect using conventional SERS sensors due to low binding affinity, were detected using a charge-selective paper-based SERS sensor by electrostatic attraction. In order to increase the affinity between the AgNPs and polar organic pollutants, two different surface charged nanoparticles were synthesized and applied to fabricate a charge-selective paper-based SERS sensor.

Chapter I. Hydrophobic modification of filter paper for highly sensitive and reproducible paper-based SERS sensor

1. Experimental section

1. 1. Chemicals and reagents

Silver nitrate ($AgNO_3$, 99.999%), sodium citrate tribasic dihydrate ($C_6H_5O_7Na_3 \cdot 2H_2O$, 99%), 4-aminothiophenol (4-ATP, C_6H_7NS, 98%) and tetramethylthiuram disulfide (thiram, $C_6H_{12}N_2S_4$, 97%) were purchased from Sigma-Aldrich (St. Louis, USA), and iron(III) dimethyldithiocarbamate (ferbam, $C_9H_{18}FeN_3S_6$, 97%) were purchased from Tokyo Chemical Industry Co., Ltd. (Tokyo, Japan). Filter paper was purchased from Advantec (grade 5C, Dublin, USA), and alkyl ketene dimer (AKD) was purchased from Solenis (Hercon-WI 155, Kimchun, Korea). All chemicals were used without further purification.

1. 2. Preparation of silver nanoparticles (AgNPs)

AgNP were synthesized by the citrate-based reduction of silver nitrate[88]. In order to synthesize of AgNP solution, the 70 mg of silver nitrate was dissolved in 400 mL of distilled water (DW). The silver nitrate solution was heated until boiling in a 3-neck round bottom flask with vigorous stirring. After boiling the silver nitrate solution, the 8 mL of 1 wt% sodium citrate solution was rapidly injected into the 3-neck round bottom flask. After 30 min further boiling, it was cooled at room temperature. To remove excess citrate in AgNP solution, the AgNP solution was centrifuged with the

condition 3000 rpm, 15 min. After centrifugation, the AgNP was dispersed in DW. The TEM image, FE-SEM image, UV/Vis extinction spectrum and size distribution of AgNP were shown in Figure 1-1. The synthesized AgNP showed a plasmonic band at 422 nm and averaged size of AgNP is 92 ± 21 nm by FE-SEM images analysis. The concentration of synthesized AgNP solution was 0.15 nM, measured by a Nanosight (LM10, Malvern, UK).

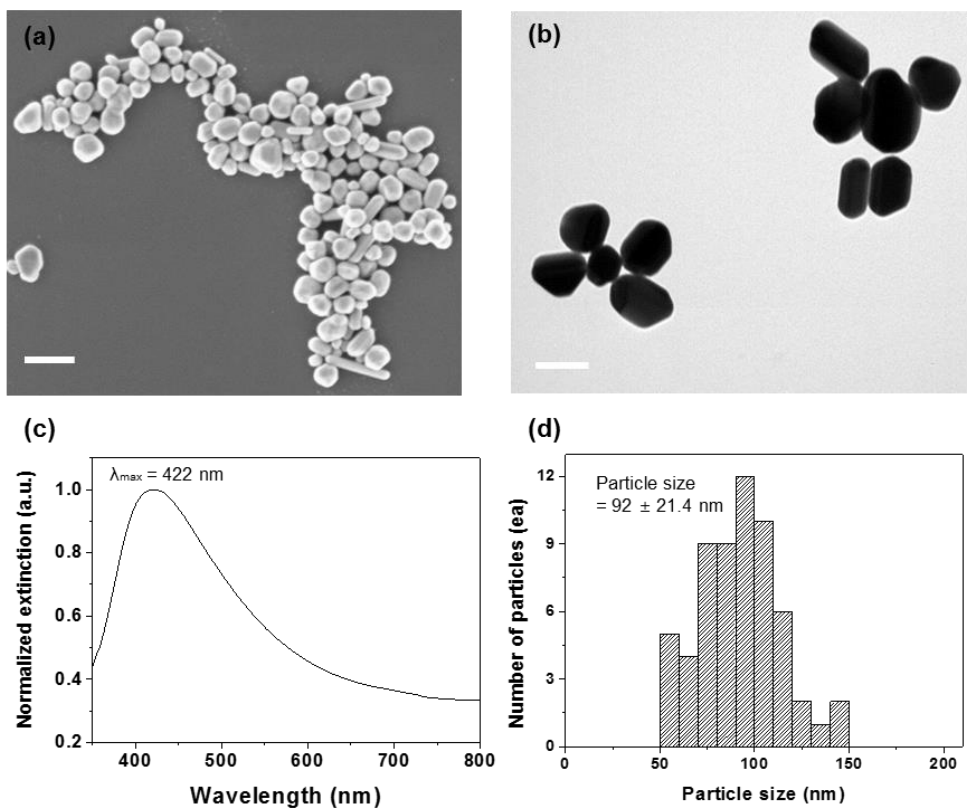

Figure 1-1. Characterization of synthesized AgNP. (a) The FE-SEM image, (b) the TEM image, (c) the UV/Vis extinction spectrum and (d) size distribution of AgNP. The scale bars represent 100 nm.

1. 3. Fabrication of hydrophobically modified filter paper

To fabricate a sensitive and reproducible filter paper–based SERS sensor, the filter paper was subjected to calendering followed by AKD treatment. An overall schematic illustration of the fabrication of the hydrophobic filter paper–based SERS sensor is shown in Figure 1-2. First, the filter paper was cut to a size of 80 mm by 50 mm. Calendering was then conducted to filter paper for reducing the roughness of the paper. For the calendering process, the paper was passed between pressing rollers. The conditions of rolling speed, calendering temperature, relative humidity and line pressure were set as 10 m/min, 23 ℃, 50% and 130 kgf/cm^2, respectively. The roughness of the filter paper was then evaluated using a Parker Print Surf (PPS) instrument (ISO 8791-4, Lorentzen & Wettre, Sweden). After calendering, the filter paper was treated with AKD as a hydrophobic agent to increase its hydrophobicity. The calendered filter paper was soaked in 0.1% AKD dispersion dissolved in DW for 2 min. After AKD treatment, the filter paper was rinsed with DW to eliminate the remaining AKD. Excess water on AKD-treated filter paper was eliminated using another filter paper, and the treated filter paper was dried using a drum drier. The temperature of the drum was 120 ℃. The contact angles of 5 μL water droplets on the bare and AKD-treated filter papers were measured by a contact angle meter (DSA100, Krüss, Germany).

1. 4. Fabrication of SERS-active AgNP spots on hydrophobically modified filter paper

For fabrication of SERS-active AgNP spots on the hydrophobic filter paper, 2 μL droplet of AgNP solution was dropped and dried on the hydrophobic filter paper at room temperature for about 1 h. After drying of the AgNP solution, 5 μL droplet of each analyte solution was dropped and dried on the AgNP spots for SERS measurement. The photographs of AgNP spots on bare filter paper and hydrophobic filter paper were shown in Figure 1-3.

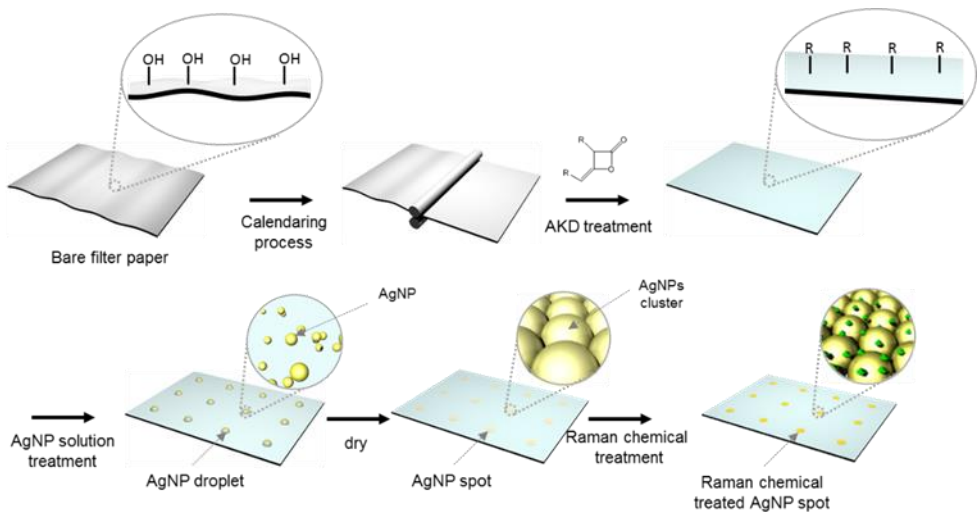

Figure 1-2. The schematic illustration of fabrication process of filter paper-based SERS sensor.

Figure 1-3. The photographs of AgNP spots on fiter papers. (a) AgNP spots on bare filter paper and (b) AgNP spots on AKD-treated filter paper.

1. 5. SERS measurement

The SERS spectra were obtained by a custom-made Raman read-out system for large-area scanning. A 643-nm laser (110-81040-019, Ondax, US) was used for the excitation source, and the output of laser power was set as 1.5 mW. The laser was delivered through a 2-axis galvanometric mirror with an area of 300 μm × 300 μm at the center of an AgNP spots using 20x objective lens (Numerical aperture (NA) = 0.40, Olympus, Japan). The scanning time of scanning area was 10 seconds. The scattered light was read by a charge-coupled device (iDus 419, Andor, UK).

1. 6. DDA calculation for theoretical E-field distributions

To investigate the dependency of SERS intensity about concentration of AgNP solution, electric field (E-field) of the AgNP nanostructure was calculated by using discrete dipole approximation (DDA, DDSCAT 7.1)[89]. The calculated structure was shown in Figure 1-4. The diameter of the AgNP was set as 80 nm, and interparticle distance between AgNPs and interdipole distance between dipoles were set as 4 nm. The dielectric constant was used value measured by Palik[90], and the surrounding medium of nanostructure was set as vacuum with refractive index of 1.00 + 0i. The incident wavelength was set as 643 nm, which was same as for the SERS measurement.

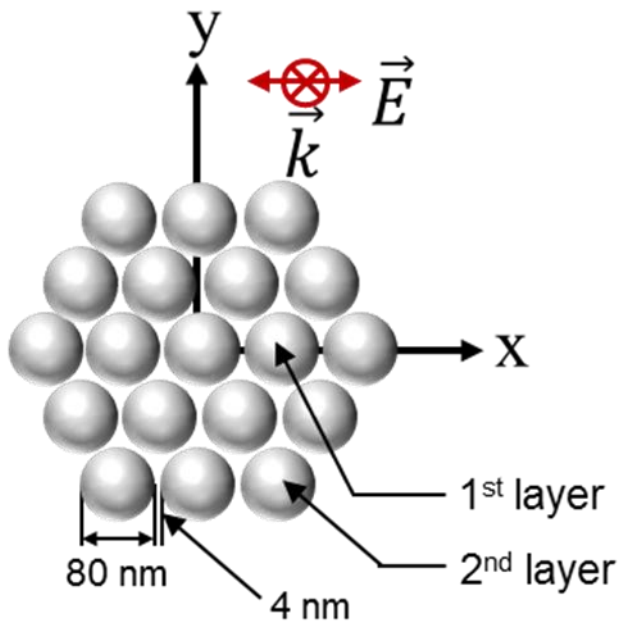

Figure 1-4. The calculated AgNP nanostructure for understanding of dependency of SERS enhancement about AgNP concentration treated on hydrophobic paper-based SERS sensors.

1. 7. Estimation of limit of detection (LOD)

To calculate limit of detection (LOD) of molecules, the log of SERS intensity versus log of concentration of analyte was linearly fitted as the followed equation.

Fitting equation:

$$\log(SERS\ intensity\ (a.u.)) = a + b \times \log(Concentration\ of\ analyte\ solution\ (nM))$$

(a: intercept, b: slope) (eq.1)

The criteria of LOD was used as $3\sigma + y_0$, and the SERS intensity of blank sample was that of AgNP spot on the hydrophobic filter paper-based SERS senser[91].

(σ: the standard deviation of SERS intensity of blank sample, y0: the SERS intensity of blank sample)

As a result, the LOD of analyte was calculated as the followed equation. LOD of analyte solution was used the equation as shown in below.

$$\log(3\sigma + y_0) = a + b \times \log(\text{LOD of analyte (nM)})$$

$$\text{LOD of analyte (nM)} = 10^{\left[\frac{\log(3\sigma + y_0) - a}{b}\right]} \quad \text{(eq. 2)}$$

2. Results and Discussions

2. 1. Hydrophobic modification of filter paper

In an effort to overcome the low sensitivity and reproducibility of conventional paper–based SERS sensors, the filter paper was treated with AKD, which changed property of filter paper from hydrophilic to hydrophobic. The aim of the hydrophobic modification was to prevent the quick absorption and to increase the retention time of aqueous solution into the filter paper. The hydrophobic modification of filter paper allowed the AgNP and analyte solutions to be retained as an aqueous droplet on the filter paper until drying within reduced contact area. These results allow to increase AgNP and analyte density on filter paper, resulted in generation of SERS hot-spot and increasing of SERS intensity of hydrophobic paper-based SERS sensor. Before surface modification of the filter paper, it was subjected to a calendering process[92] to reduce the surface roughness of filter paper. For calendering process, filter paper was passed between two rolls at high pressure and temperature to reduce its roughness. Through the calendering process, the PPS roughness of the filter paper was reduced from 9.4 μm to 4.0 μm, as shown in Figure 1-5a. After calendering, the filter paper was immersed into AKD solution to allow esterification reaction of AKD with the hydroxyl groups of the cellulose fibers in the filter paper. Through the AKD treatment, the cellulose fibers were functionalized with alkyl groups, which modified

the nature of the filter paper from hydrophilic to hydrophobic. To verify the hydrophobic modification of the filter paper, the contact angles of filter paper before and after AKD treatment were measured, as shown in Figure 1-5b. The contact angle of a water droplet on bare filter paper was 15°, and the droplet was immediatly absorbed into the paper. However, the contact angle of a water droplet on AKD-treated filter paper was increased to 114°, and the droplet was retained on the surface of the paper for 1 h until drying. As a consequence, the AgNP and analyte solutions could be retained within a small area of the filter paper surface for a longer time.

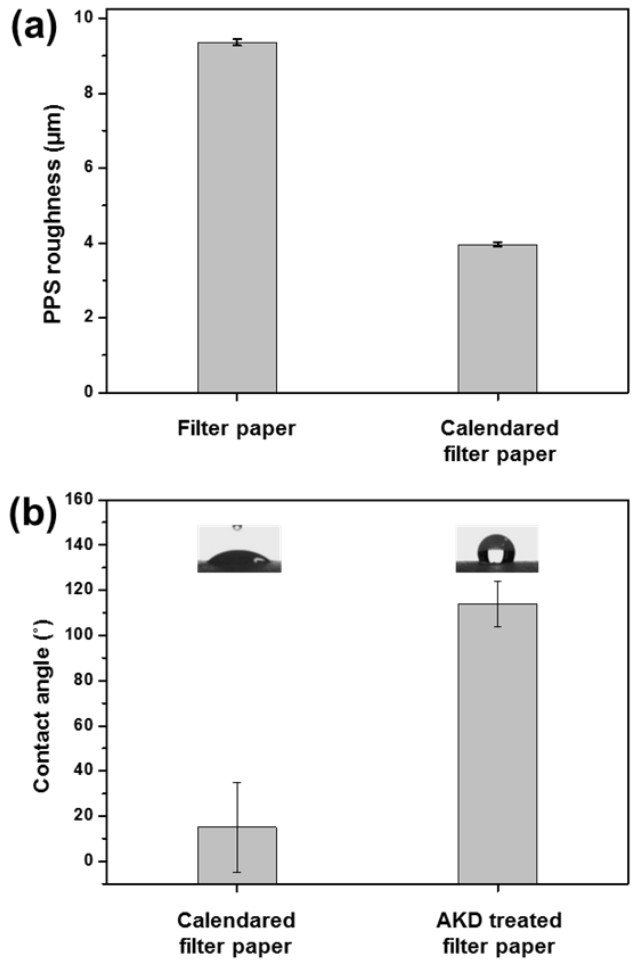

Figure 1-5. Characterization of surface properties of filter papers. (a) Surface roughness analysis of filter paper and calendered filter paper. (b) Contact angles of calendered filter paper and AKD-treated filter paper. Inset photographs were water droplets on each filter paper, respectively.

To investigate the effect of hydrophobic modification on the SERS activity of AgNP spots on the filter papers, 4-ATP was used as a test analyte. To evaluate the SERS intensity of each filter paper, the AgNP solution was dropped and dried to form SERS active spots on the surface of filter paper and AKD-treated filter paper, and then, 5 μL of 1 μM 4-ATP solution was dropped and dried on each SERS active spot.

The AgNP distribution and SERS spectrum of each filter paper were shown in Figure 1-6. Bare filter paper was showed low SERS intensity because of low AgNP density on filter paper. However, the hydrophobic filter paper was showed highly enhanced SERS intensity because of high AgNP density on AKD-treated filter paper. These phenomena were originated that hydrophobic modification of filter paper confined AgNP solution within small contact area by increasing contact angle of aqueous solution. By reduced contact area of AgNP solution, the density of AgNP was increased, and the AgNPs was formed small AgNP clusters, resulted in creating SERS hot-spots. As a result, the SERS intensity of AKD-treated filter paper was highly enhanced. These results confirmed that hydrophobic modification of the paper surface successfully promoted the SERS intensity of the filter paper–based SERS sensor.

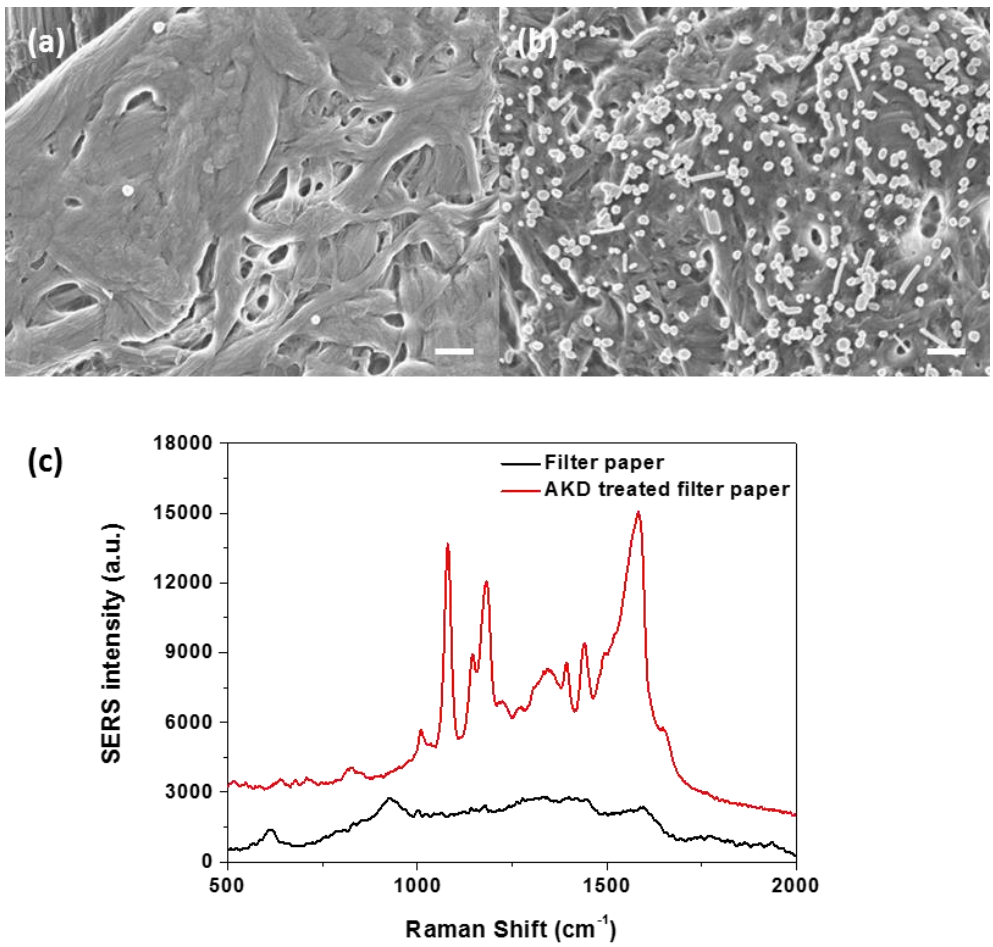

Figure 1-6. Characterization of surface and SERS intensity depending on modification of filter paper. The FE-SEM images of (a) AgNP spots on filter paper and (b) AgNP spots on AKD-treated filter paper. (c) The SERS spectra of AgNP spots on filter paper and AKD-treated filter paper treated by 5 μL of 1 μM 4-ATP solution. The scale bar was set as 100 nm.

2. 2. Control of AgNP distribution of paper-based SERS sensor for SERS intensity optimization

Because SERS enhancement is affected by the distribution and conformation of nanoparticles[64, 77], to optimize the SERS enhancement of the hydrophobic filter paper–based SERS sensor, the SERS enhancements were compared as a function of the concentrated ratios of the AgNP solutions. To evaluate the SERS enhancement, the AgNP solutions of various concentrations were dropped and dried on surface of hydrophobic filter paper. After drying of the AgNP solution, 5 μL of 1 μM 4-ATP solution was dropped on the each AgNP spot, and the SERS spectrum of each AgNP spot on hydrophobic filter paper was measured.

Figure 1-7 showed the AgNP distributions depending on the concentrated ratios of the AgNP solutions on the hydrophobic filter paper. The concentration of synthesized AgNP solution was 0.15 nM, and called as reference solution. The concentrated ratios of AgNP solutions were set as 2.5, 5, 10, 20 and 40 times, which concentrations were corresponded 0.375, 0.75, 1.5, 3.0 and 6.0 nM, respectively. As the concentrated ratio of the AgNP solution was increased up to 10 times, the density of AgNP increased and the AgNP clusters grew larger, formed a large structure on the surface of hydrophobic filter paper. However, as the concentrated ratio of the AgNP solution was increased to more than 10 times, the AgNP formed multilayer and three-dimensional aggregated AgNP structure, which were larger than several micrometers

on the surface of hydrophobic filter paper. For comparison of the SERS enhancement with different concentrated ratios of AgNP solutions, the SERS intensity 1073 cm^{-1} band of 4-ATP on each AgNP spot with different concentrated ratio on hydrophobic filter paper was used for the SERS enhancement. The SERS spectrum and SERS intensity of 1073 cm^{-1} band of 4-ATP on each AgNP spot were shown in Figure 1-8 and Figure 1-9, respectively. The SERS intensity of the 1073 cm^{-1} band was gradually increased as the concentrated ratio of the AgNP solution was increased, and maximized when the concentrated ratio of the AgNP solution was 10 times. However, the SERS intensity slightly decreased as the concentrated ratio of AgNP solution was increased more than 10 times.

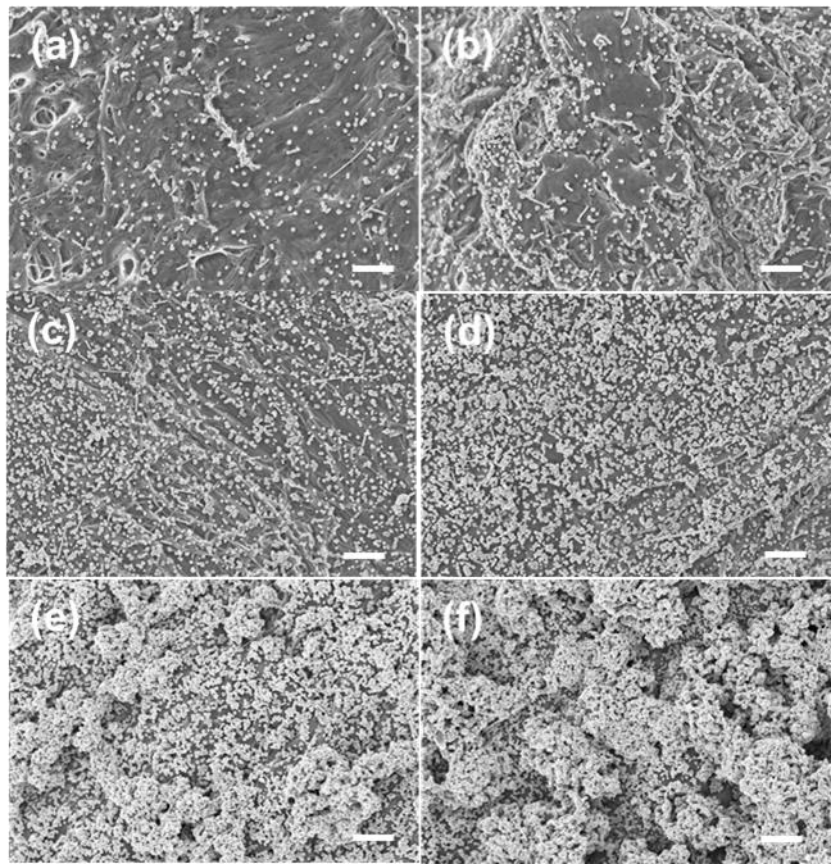

Figure 1-7. The AgNP distributions depending on concentration of AgNP on hydrophobic filter paper. The FE-SEM images of (a) not concentrated AgNP solution (reference AgNP solution, 0.15 nM), (b) 2.5 times concentrated (0.37 nM), (c) 5 times concentrated (0.75 nM), (d) 10 times concentrated (1.5 nM), (e) 20 times concentrated (3.0 nM), and (f) 40 times concentrated (6.0 nM) AgNP solution.The scale bar was set as 1000 nm.

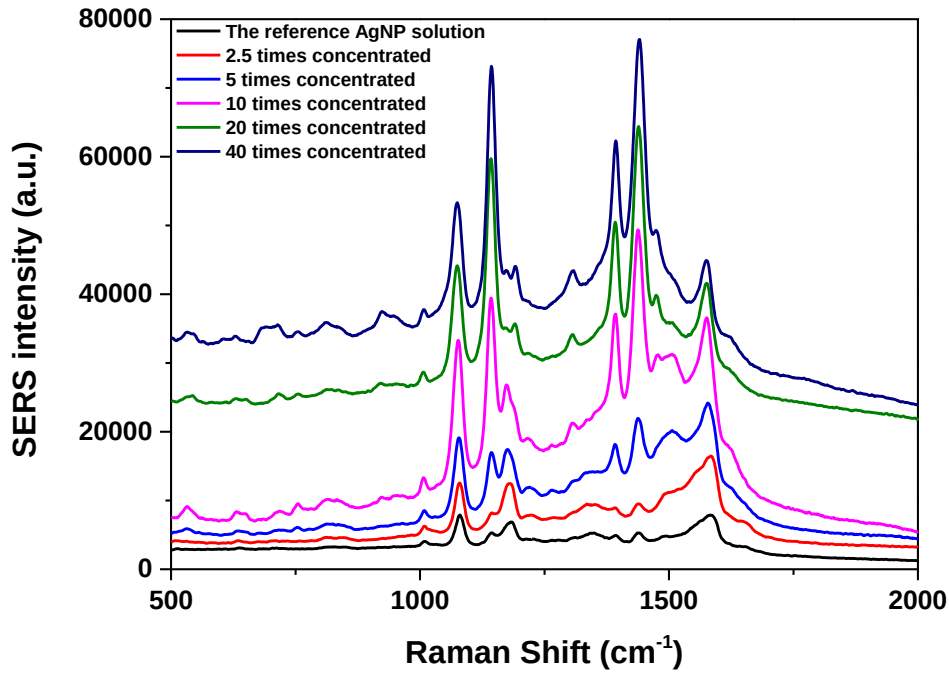

Figure 1-8. The SERS spectra of 4-ATP treated on each AgNP spot with different concentrated ratios of AgNP solution from 1 to 40 times. Each AgNP spot was treated with 5 μL of 1 μM of 4-ATP solution.

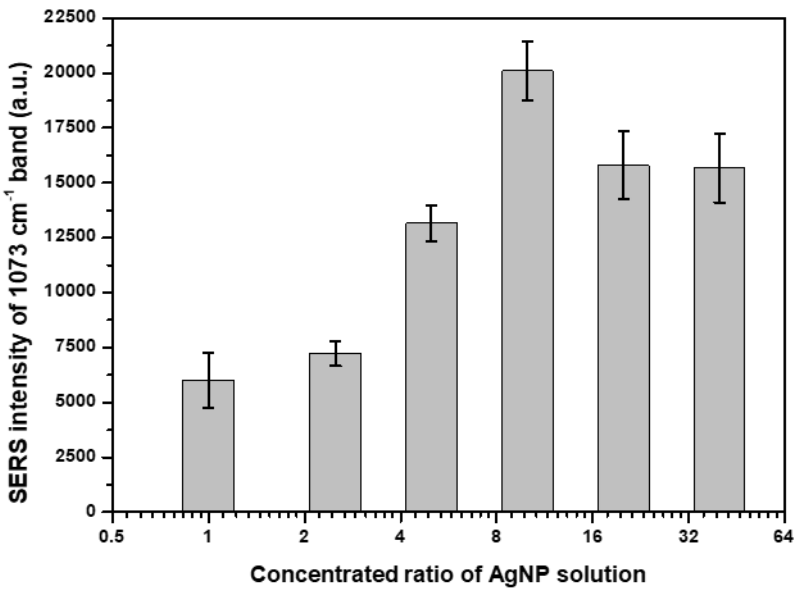

Figure 1-9. The graph of SERS intensities of 1073 cm^{-1} band of 4-ATP versus concentrated ratios of AgNP solutions. Each AgNP spot on AKD-treated filter paper was treated with 5 μL of 1 μM 4-ATP solution.

To investigate variation of SERS intensity depending on concentrations of AgNP, E-field distributions of AgNP clusters with different number of AgNP layers were calculated by DDA[89]. E-field distributions and maximum E-field intensities of those structures were shown in Figure 1-10 and Figure 1-11. To identify the effect of the size of the AgNP clusters on the E-field intensity, a series of AgNP clusters was considered, as shown in Figure 1-4. The increase of size of AgNP cluster resulted in an increase in the number of AgNP layers in the calculated nanostructures. As the size of the AgNP clusters was increased, the maximum E-field intensity also increased. However, as the cluster size was increased beyond the optimal value, the maximum E-field intensity was steadily decreased as the number of AgNP layers in the clusters more than two. The decrease in E-field intensity was caused by delocalization of the E-field as the AgNP clusters grew larger. With small AgNP clusters, the E-field was concentrated between AgNPs, which enhanced the maximum E-field intensity. However, as the number of AgNP layers was increased, the E-field of AgNP nanostructure became delocalized throughout the larger structures, and maximum E-field intensity was decreased[64, 93]. This was consistent with the variation of SERS enhancement depending on concentrated ratio of AgNP solution. For that reason, as the concentrated ratio of AgNP solution was increased, the size of AgNP cluster was increased, resulted in decreasing of SERS intensity because of delocalization of E-field in AgNP cluster. In addition, vertically piled

structures of nanoparticles showed decreasing of SERS intensity due to the delocalization of optical field as well as hindrance of irradiation and the scattering of light[77]. As a results, it was shown that the optimal concentration of AgNP solution for fabrication of AgNP spots was 1.5 nM, which was corresponded with concentrated ratio of 10 times of AgNP solution.

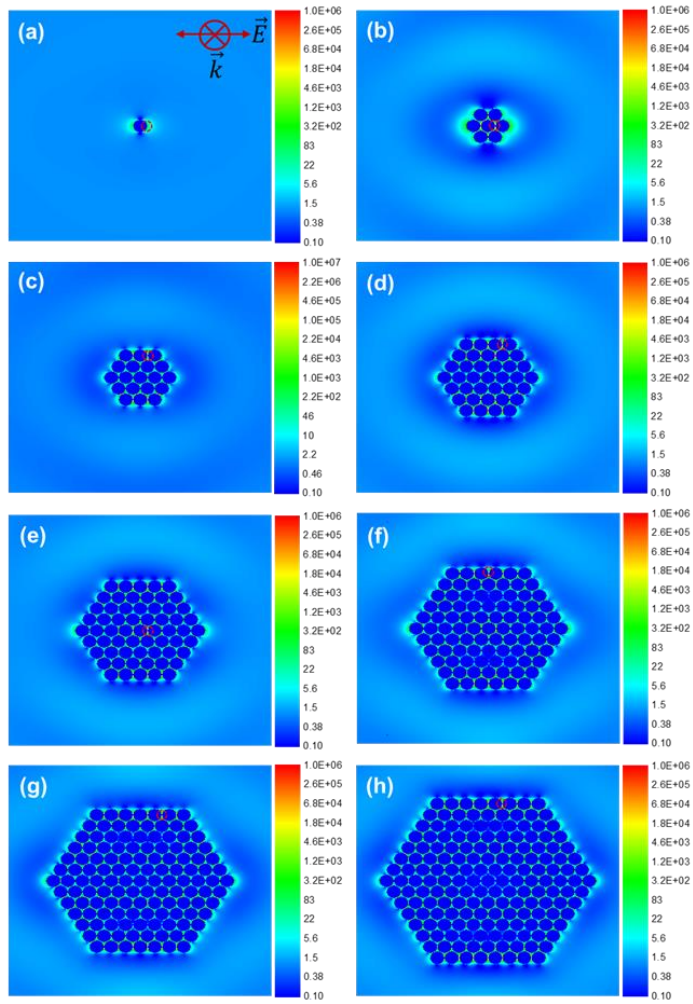

Figure 1-10. The calculated electric field (E-field) distributions of AgNP clusters by discrete dipole approximation (DDA) method: (a) Monomer, (b) 1 layer, (c) 2 layers, (d) 3 layers, (e) 4 layers, (f) 5 layers, (g) 6 layers and (f) 7 layers of AgNP around the center one. The red line means location of maximum E-field intensity.

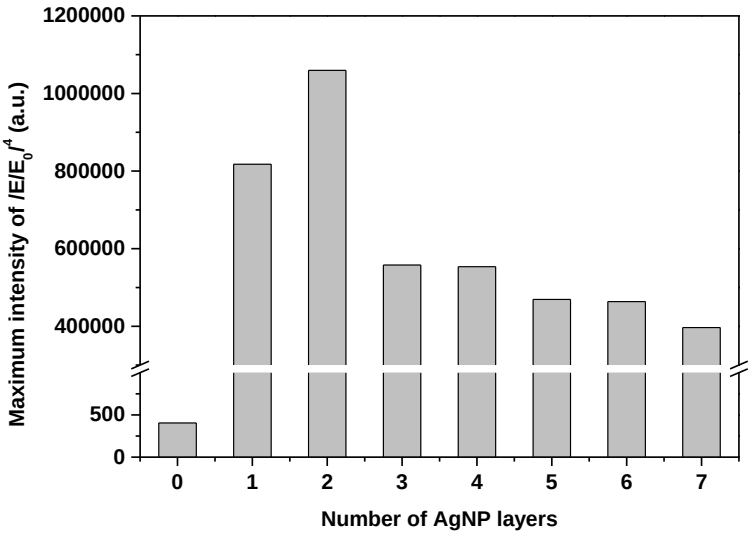

Figure 1-11. The maximum E-field intensities versus number of AgNP layers in AgNP clusters.

2. 3. Reproducibility and sensitivity test of paper based-SERS sensor

High reproducibility and sensitivity are important criteria for SERS sensor. At first, to evaluate the reproducibility of the hydrophobic filter paper–based SERS sensor, the SERS spectra of 25 AgNP spots treated with 5 μL of 1 μM 4-ATP solution were measured. To measure the reproducibility, the spot-to-spot variation of SERS intensity was quantified by the 1073 cm^{-1} band of 4-ATP on the hydrophobic filter paper-based SERS sensor. The SERS spectra and SERS intensities of the 1073 cm^{-1} band of 4-ATP on AgNP spots were shown in Figure 1-12. The RSD of the SERS intensities of the 1073 cm^{-1} band of 4-ATP among the 25 AgNP spots was calculated as 6.19%, slightly higher than or similar to those of previous studies[76, 94-95]. The high reproducibility evidently originated from the hydrophobic modification of the filter paper, which prevented the aqueous AgNP solution from absorption into the filter paper and allowed the AgNP to be uniformly retained on the surface of the paper. Furthermore, the large area scanning system combined with micro Raman was also affected to increase the reproducibility of paper-based SERS sensor because this Raman system was averaged the SERS signal over the scanning area. As a result, it was confirmed that the RSD of SERS intensity of the hydrophobic filter-paper based SERS sensor was increased up to 6 % by combining of sensor and measurement effect.

To evaluate the sensitivity of the hydrophobic filter paper–based SERS sensor, the SERS spectra of AgNP spots treated with 5 μL droplets of 4-ATP with concentrations from 0.1 nM to 1000 nM were measured, as shown in Figure 1-13a. The SERS spectrum of each concentration was obtained from 7 AgNP spots. The averaged SERS intensities of the 1073 cm^{-1} band of 4-ATP with different 4-ATP concentrations were shown in Figure 1-13b. The SERS intensity of 4-ATP decreased as the concentration of 4-ATP was decreased, and it is hard to detect below 1 nM. The LOD of 4-ATP using the hydrophobic filter paper–based SERS sensor was estimated by linear fitting of the SERS intensities versus concentrations of 4-ATP, as shown in Figure 1-14 and Table 1-1. The calculated LOD of 4-ATP using this sensor was 0.603 nM. Furthermore, to evaluate the stability of the hydrophobic filter paper-based SERS sensor, we collected the SERS spectra of AgNP spots treated with 5 uL of 1 uM 4-ATP solution during 15 days as shown in Figure 1-15. The SERS intensity of 1073 cm^{-1} band of 4-ATP was decreased in a few days and reached a plateau there. After 5 days, the SERS intensity was maintained with the 15% decreasing of SERS intensity compared with freshly prepared SERS sensor.

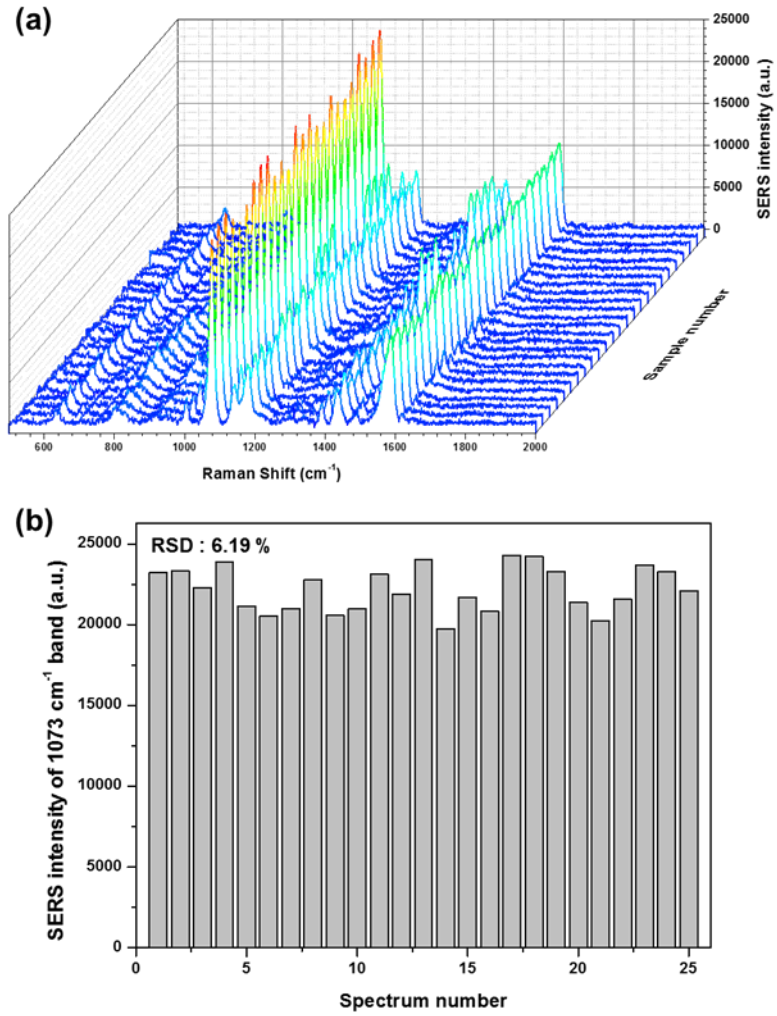

Figure 1-12. The reproducibility of hydrophobic filter paper-based SERS sensor. (a) The SERS spectra of 25 AgNP spots treated with 5 μL of 1-μM 4-ATP solution, and (b) the SERS intensities of 1073 cm^{-1} band of 4-ATP of 25 AgNP spots.

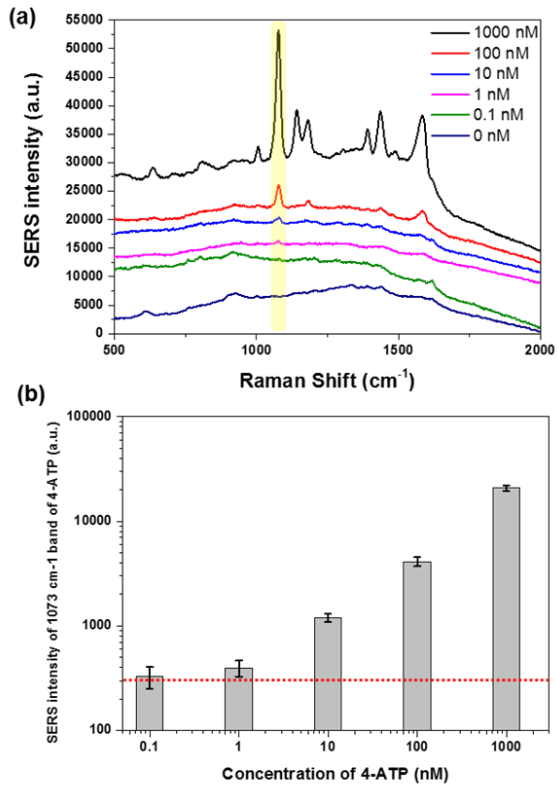

Figure 1-13. The sensitivity of hydrophobic filter paper-based SERS sensor. (a) The SERS spectra of AgNP spots treated with different concentrations of 4-ATP from 0 nM to 1000 nM. (b) The SERS intensities of 1073 cm^{-1} band of 4-ATP with different concentrations of 4-ATP from 0.1 nM to 1000 nM. Each SERS intensity was averaged from 7 AgNP spots. The error bars represent standard deviations. The dotted red line means SERS intensity of AgNP spots, which was blank sample (= 0 nM of 4-ATP).

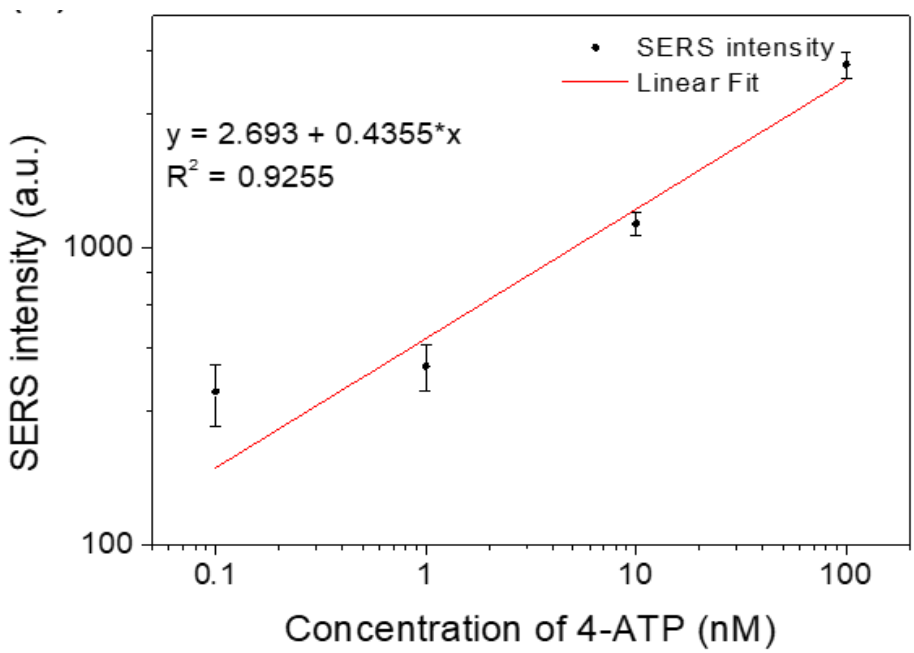

Figure 1-14. The linear fitting of SERS intensities versus concentrations of 4-ATP to calculate LOD of 4-ATP by using the hydrophobic filter paper-based SERS sensor.

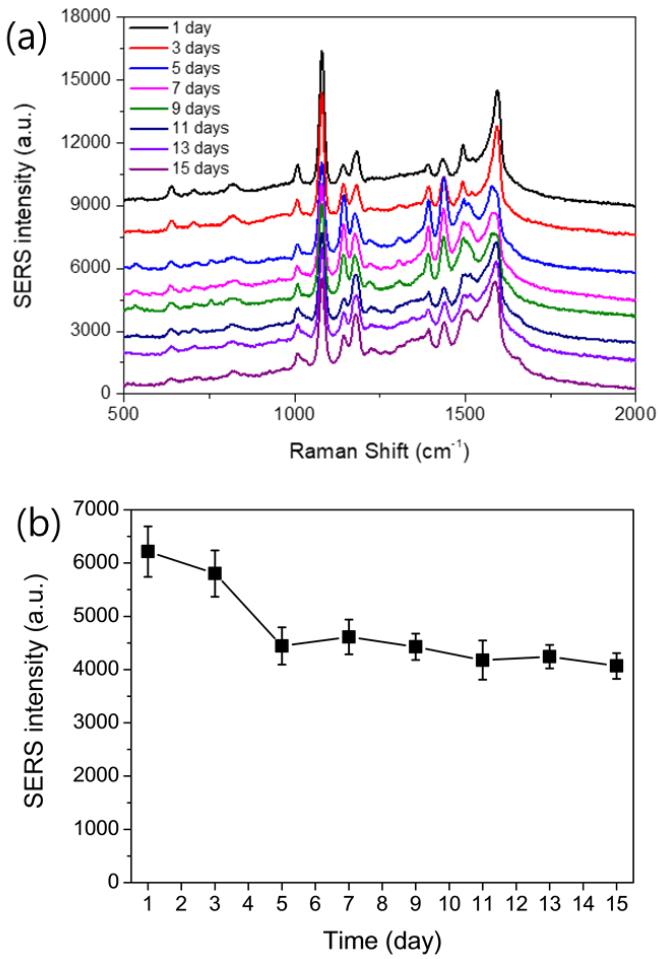

Figure 1-15. The stability of the hydrophobic filter paper-based SERS sensor. (a) The SERS spectra of hydrophobic filter paper-based SERS sensor during 15 days and (b) the SERS intensity of 1073 cm^{-1} band of 4-ATP treated on the hydrophobic filter paper-based SERS sensor. The hydrophobic filter paper-based SERS sensor was treated by 5 μL of 1 μM of 4-ATP solution.

2. 4. Application to pesticides detection

To confirm its applicability to detection of actual pesticides, the hydrophobic filter paper-based SERS sensor was used to analyze thiram and ferbam. For this procedure, the SERS spectra of AgNP spots treated with 5 μL droplets of solution of pesticides were measured. Both pesticides was dissolved in DW, and the concentrations of pesticides were varied from 0.1 nM to 10000 nM, as shown in Figure 1-16a and 1-16b. The averaged SERS intensities at 1400 cm^{-1} with different concentrations of pesticides were shown in Figure 1-165c and 1-16d. These SERS intensities were collected from 10 AgNP spots on the hydrophobic filter paper-based SERS sensor. Analysis of the SERS spectra as a function of the concentrations of pesticides confirmed that thiram and ferbam could be detected at the nanomolar level, as shown in Figure 1-16a and 1-16b. Furthermore, the LODs of thiram and ferbam, estimated by linear fitting of the SERS intensity versus concentrations of each pesticide, were 0.461 nM and 0.491 nM, respectively, as shown in Figure 1-17 and Table 1-1. These results confirmed that the SERS sensor based on hydrophobic filter paper-based SERS sensor can be applied to the detection of trace amounts of pesticides at the sub-nanomolar level.

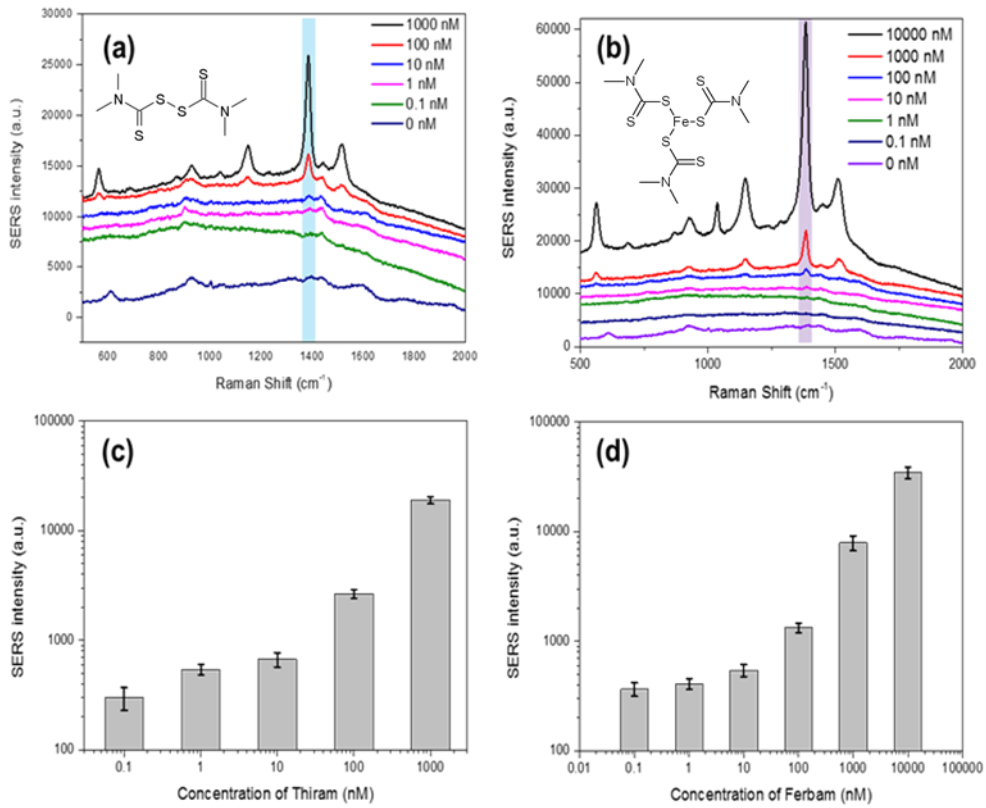

Figure 1-16. The application to measurement of pesticides using the hydrophobic paper-based SERS sensor. The SERS spectra of hydrophobic filter paper-based SERS sensors treated with different concentrations of (a) thiram and (b) ferbam from 0 nM to 10000 nM. The SERS intensities of 1400 cm^{-1} band of (c) thiram and (d) ferbam versus concentrations of pesticides. Each SERS intensity was averaged from 10 AgNP spots. The error bars represent standard deviations.

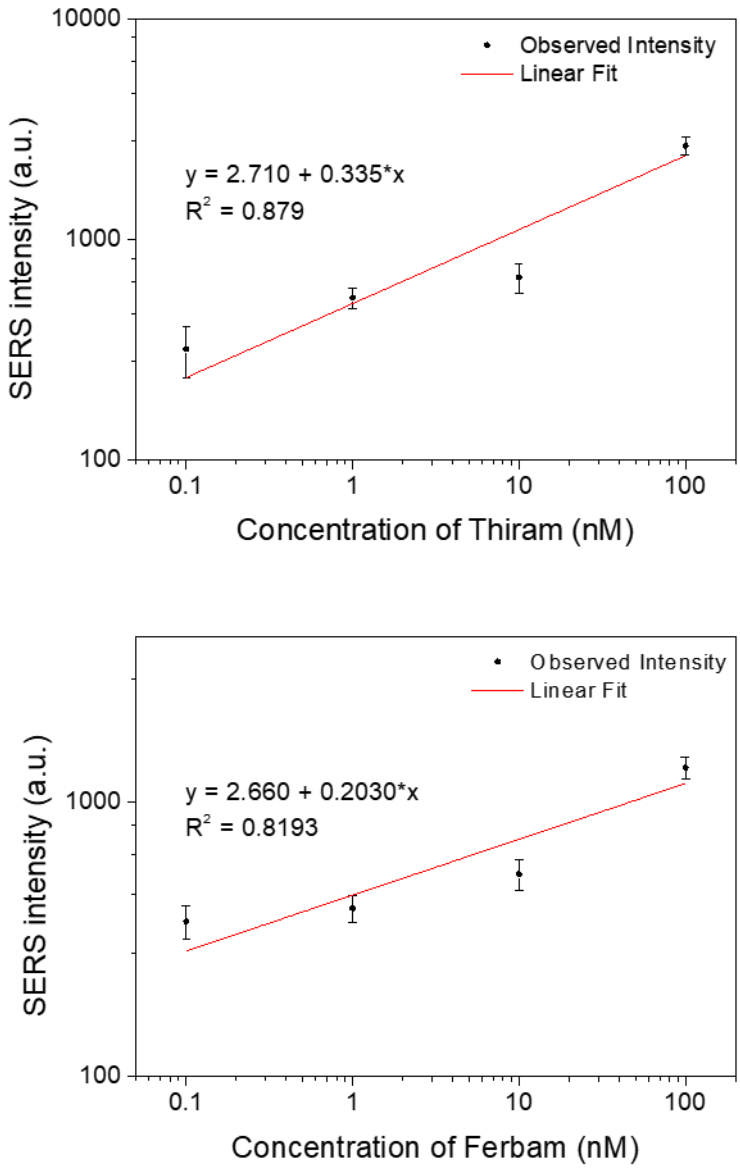

Figure 1-17. The linear fittings of SERS intensity versus concentration of thiram (upper) and ferbam (lower) to calculate LODs.

Sample	a (intercept of fitted line)	b (slope of fitted line)	σ (Standard deviation of SERS intensity of blank sample)	y_0 (SERS intensity of blank sample)	R^2	LOD (nM)
4-ATP	2.693	0.4355	63.986	203.680	0.926	0.603
Thiram	2.710	0.3350	63.986	203.680	0.879	0.461
Ferbam	2.660	0.2030	63.986	203.680	0.819	0.491

Table 1-1. Estimation of limits of detections (LODs) of analytes.

Chapter II. Surface roughness reduced paper-based SERS sensor by introducing cellulose nanofibrils (CNF) on paper for increasing reproducibility

1. Experimental

1. 1. Chemicals and reagents

Silver nitrate ($AgNO_3$, 99.999%), sodium citrate tribasic dihydrate ($C_6H_5O_7Na_3 \cdot 2H_2O$, 99%), 4-aminothiophenol (4-ATP, $H_2NC_6H_4SH$, 99%), and rhodamine 6G (R6G, $C_{28}H_{31}N_2O_3Cl$, 99%) were purchased from Sigma-Aldrich (St. Louis, MO, USA). Filter paper was used as a substrate (5C, Advantec, Tokyo, Japan). The AKD was purchased from Solenis (Hercon-WI 155, Kimchun, Korea). The carboxymethyl cellulose (CMC) was purchased from CP Kelco Korea (DS 0.78, Finnfix 5, Seoul, Korea). A bleached eucalyptus kraft pulp was purchased from Moorin P&P (Seoul, Korea). All chemicals were used without further purification.

1. 2. Preparation of cellulose nanofibrils (CNF) coated hydrophobic filter paper

To increase the uniformity of the paper-based SERS sensor, CNF suspension containing a small amount of CMC was applied to filter paper. CMC was used to control the rheological properties of the cellulose nanofibrils (CNF) suspension. A bleached eucalyptus kraft pulp (Moorim P&P, Ulsan) was grinded with a grinder (Super Masscolloider, Masuko Co., Japan) to prepare the CNF. After that, the grinded pulp was treated by a laboratory valley beater to fibrillated CNF from pulp.

The photograph of pulp and TEM image of the CNF were shown in Figure. 2-1. Most CNFs were less than 50 nm in width but less fibrillated bundle were also existed more than 100 nm.

In order to apply CNF to filer paper surface, the mixture of 10 mL of CNF and CMC was applied to the hydrophobic filter paper surface, which have 15 cm × 30 cm in size. The concentration of CNF and CMC in suspension was 1 wt% and 0.03 wt%, respectively. The prepared CNF suspension mixed with CMC was applied onto the hydrophobic filter paper with a laboratory bar coater (Auto Bar Coater, GIST, Korea) with wire bar (Bar No. 14). After the CNF coating on filter paper, the CNF coated filter paper was dried under the 120 ℃, overnight. After drying, to maintain hydrophobicity of CNF coated filter paper for sensitive SERS detection, the CNF coated filter paper was treated by AKD solution because the coated CNF had hydrophilic nature by hydroxyl group in CNF.

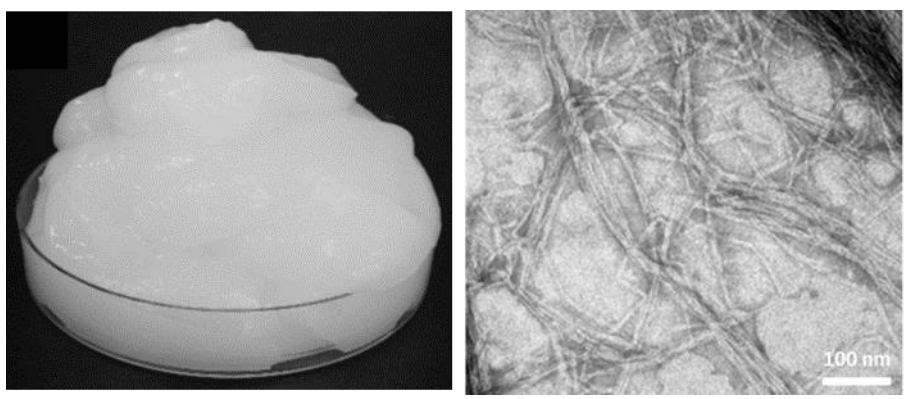

Figure 2-1. The photograph of pulp (left) and TEM image of the CNF (right).

1. 3. Fabrication of SERS-active AgNP spots on CNF coated filter paper

To fabricate the SERS-active AgNP spots on the CNF coated hydrophobic filter paper, the 2 μL of AgNP solution was dropped and dried on filter papers, which applied different number of CNF coatings. And then, the filter papers were dried at room temperature for about 1 h. After drying of the AgNP solution, the 5 μL of analyte solution was dropped and dried on the AgNP spots for SERS measurement.

1. 4. SERS measurement

The SERS spectra were obtained by a custom-made large-area Raman scanning system combined with micro Raman system. The excitation source was used a 643-nm laser (110-81040-019, Ondax, US), and the laser power was 1.5 mW. The irradiated and scattered light was collected through 10x (NA=0.25, Olympus, Japan), 20x (NA=0.40, Olympus, Japan) and 40x (NA=0.75, Olympus, Japan) objective lens. The scanning area were 600 μm × 600 μm (10x objective lens), 300 μm × 300 μm (20x objective lens) and 200 μm × 200 μm (40x objective lens). The acquisition time was 10 seconds. The scattered light was read by a charge-coupled device (iDus 419, Andor, UK).

2. Results and Discussion

2. 1. Effect of numerical apertures on sensitivity and reproducibility of paper-based SERS sensor

The sensitivity of SERS sensor was affected by the value of NA of objective lens because the solid angle of light and confocal volume were affected by NA. In addition, the SERS signal was increased as the value of NA was increased[96-97]. To confirm the change of confocal volume according to value of NA, The calculated confocal volumes with different values of NA were calculated as shown in Figure 2-2 for comparison of changing of confocal volume by value of NA[98]. As the value of NA was increased, the confocal volume was decreased because the focal length and beam size were decrease. However, the intensity of scattered light by objective lens was increased because of increasing of solid angle. These tendencies indicated that the SERS intensity was increased as the value of NA was increased, however, the reproducibility of filter paper-based SERS sensor was decreased as the value of NA was increased. Despite of the increasing SERS intensity by the high value of NA, the reproducibility of SERS intensity was decreased because the height dependency of the SERS measurement was increased due to small focusing volume. By nature of filter paper, the numerous pores and high surface roughness of filter paper was reduced the reproducibility of paper-based SERS sensor with high value of NA as

shown in Figure 2-3.

To investigate the effect of NA on the SERS signal in hydrophobic filter paper-based SERS sensor, the SERS spectra of the hydrophobic paper-based SERS sensor treated with 5 μL of 1 μM R6G were measured through the objective lens with different values of NA. The SERS spectra and average SERS intesities of 1510 cm^{-1} band of R6G were shown in Figure 2-3a and 2-3b. For the SERS measurements, the value of NA of objective lens were used 0.25, 0.40, 0.75, respectively. As the value of NA were increased, the SERS intensity dramatically increased. However, the reproducibility of SERS intensity was reduced as shown in Figure 2-3c. Each RSD was obtained from 7 different AgNP spots. The RSDs of SERS intensities with values of NA of 0.25, 0.40, 0.75 were 8.7%, 10.9% and 26.7%, respectively. These tendencies meant that it was necessary to measure using objective lens with high NA for highly sensitive SERS detection. However, the current paper-based SERS sensor showed low reproducibility originated by high surface roughness and non-uniform surface of filter paper. As a result, to realize highly sensitive SERS dection with objective lens with high NA, paper-based SERS sensor with improved roughness and uniformity of surface should be manufactured.

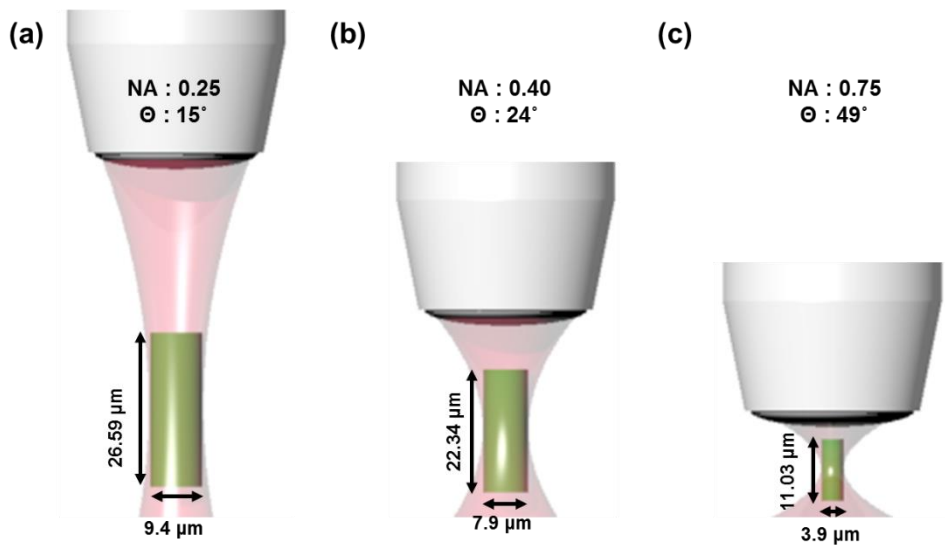

Figure 2-2. The illustrations of light irradiation and theoretical effective confocal volume with different values of NA. (a) NA: 0.25, (b) NA: 0.40, and (c) NA: 0.75. Inset cylinder of irradiated light of illustration was theoretical conforcal volume.

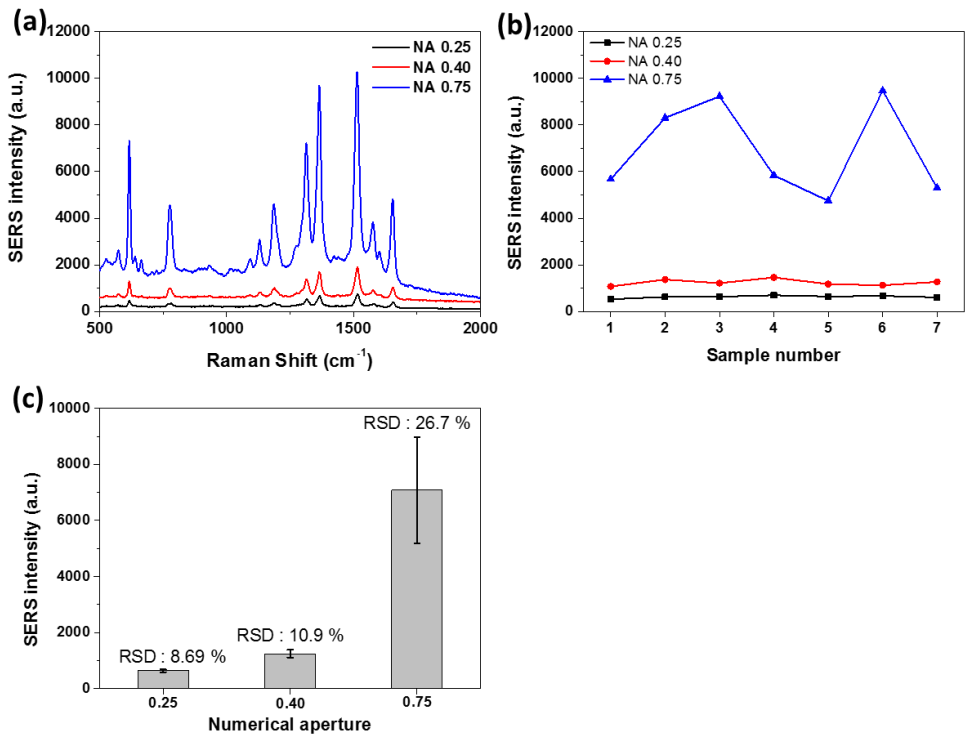

Figure 2-3. Characterization of SERS signals of hydrophobic filter paper-based SERS sensor with different values of NA. (a) The SERS spectra of AgNP spots with different NAs. (b) The SERS intensity of 1510 cm^{-1} band of R6G on each AgNP spot with different NAs. (c) The averaged SERS intensities of 1510 cm^{-1} band of R6G with different values of NA.

2. 2. Analysis of surface morphology of CNF coated paper-based SERS sensor

To improve surface uniformity of filter paper, the CNF coating was applied to the hydrophobic filter paper. The CNF was a nanosize cellulose fibrils which produced by differentiating pulp. By applying CNF to surface of filter paper, the nanosize CNF filled the surface of filter paper. As a result, the pores and surface roughness of filter paper were reduced. The schematic illustration of effect of CNF coating on filter paper was shown in Figure 2-4. In addition, the structure of CNF was same with cellulose fibrils in the paper because the components of both were same. As a result, the CNF was not affected the backgound SERS signal. Thus, the CNF was a suitable material for increasing surface uniformity of filter paper.

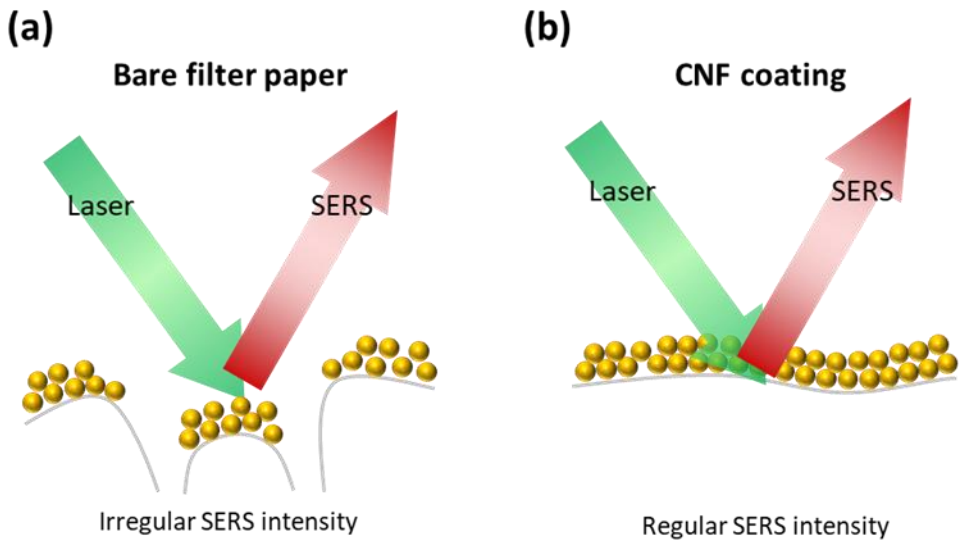

Figure 2-4. The schematical illustration of filter paper-based SERS sensors. (a) The hydrophobic filter paper–based SERS sensor and (b) the CNF coated the hydrophobic filter paper-based SERS sensor.

When the CNF coating was applied to the hydrophobic filter paper, the CMC was added to CNF solution for controlling the rheology of the CNF solution on the hydrophobic filter paper by increasing the viscosity of the CNF suspension. In addition, the previous research showed that the addition of CMC improved the dispersing of CNF by disentangling the nanofibrils and increasing the anionic charge in the suspension[99]. By these reasons, CMC was added to CNF solution. This dispersion of CNF on paper surface resulted in the formation of uniform paper surface by filling the pores and reducing surface roughness of filter paper. After CNF coating on hydrophobic filter paper, the CNF coated filter paper was applied to AKD treatment for maintaining the hydrophobic property of filter paper for highly sensitive SERS detection. The FE-SEM images of filer papers with different number of CNF coatings were shown in Figure 2-5. As shown in Figure 2-5, uniformity of the paper surface was improved by applying CNF coatings. Many large pores remained on the CNF untreated filter paper, however, the most of the pores was disappeared, and the surface smoothness was improved with the CNF coating because the overall surface roughness was flattened by the filled CNF.

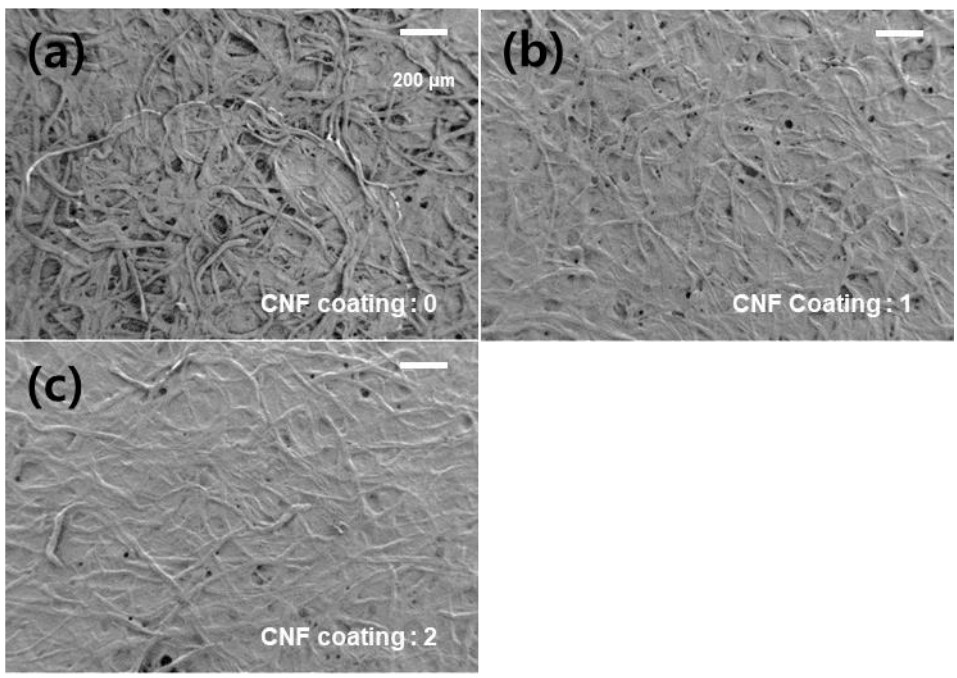

Figure 2-5. The characterization of surface morphology change of hydrophobic filter paper by CNF coating. The FE-SEM images of hydrophobic filter papers with different number of CNF coatings. (a) CNF untreated, (b) one CNF coating and (c) double CNF coating on hydrophobic filter paper.

To identify the effect of CNF coating on uniformity of filter paper-based SERS sensor, the distribution and converage of AgNP on each AgNP spot were analyzed by FE-SEM images. The FE-SEM images of AgNP spots on hydrophobic filter papers were shown in Figure 2-6. As the number of CNF coatings on the hydrophobic filter paper was increased, the AgNP spot became more circular and AgNP distribution was more uniform. In addition, overall surface roughness and the number of pores of hydrophobic filter paper were decreased by CNF coating.

To analysis coverage of AgNP on AgNP spot, the FE-SEM images of AgNP spots were analyzed by area of pores in overall AgNP spot. The coverage of AgNP was calculated by the eq. 3.

$$\text{The surface coverage of AgNP on AgNP spot} = \frac{\text{AgNP covered area}}{\text{AgNP spot area}} \quad \text{(eq. 3)}$$

The AgNP overage of AgNP spot was shown in Figure 2-7. The coverage of AgNP of AgNP spot was increased as the number of CNF coatings was increased because the surface roughness and pores on surface of filter paper were reduced by CNF coating. Thus, CNF coating to hydrophobic filter paper reduced the pore and flattened surface roughness of surface of filter paper. As a result, CNF coating made more uniform AgNP spots on filter paper-based SERS sensor for increasing reproducibility of filter paper-based SERS sensor.

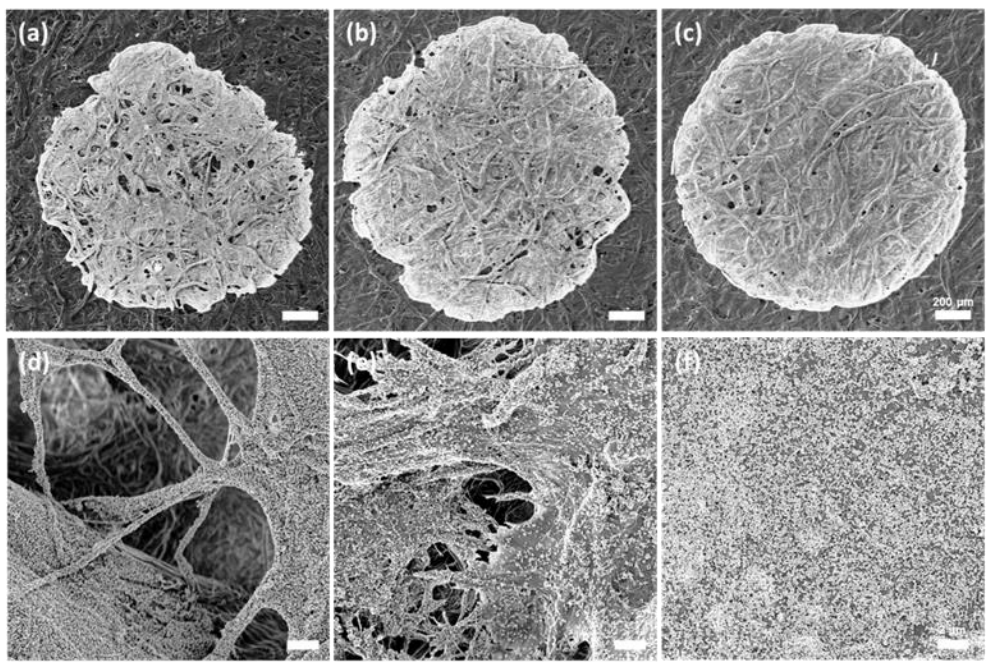

Figure 2-6. Characterization of AgNP spots on hydrophobic filter paper with different number of CNF coatings. FE-SEM images of AgNP spots on (a) CNF untreated, (b) one CNF coating and (c) double CNF coatings on hydrophobic filter paper. High magnified FE-SEM images of AgNP spots on (d) CNF untreated, (e) one CNF coating and (f) double CNF coatings on hydrophobic filter paper. The scale bars of (a) – (c) were 200 μm and those of (d) – (f) were 2 μm.

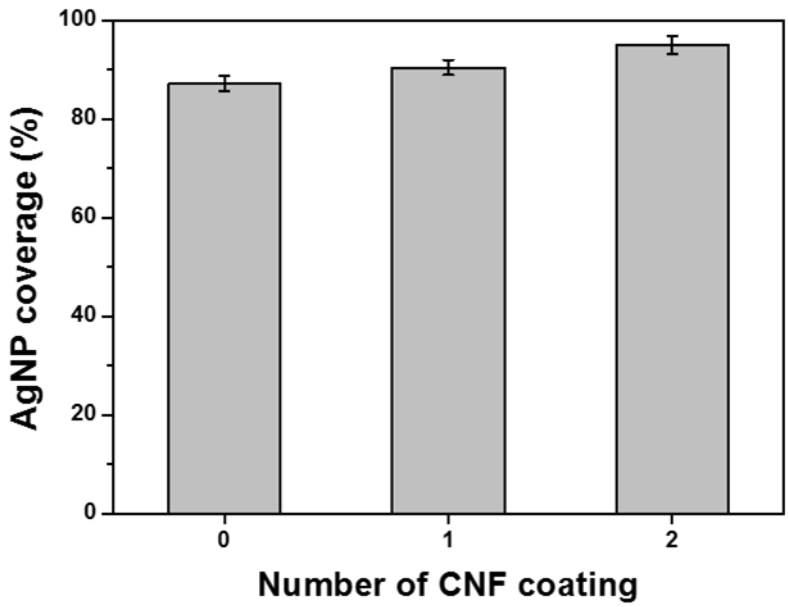

Figure 2-7. The AgNP coverage on AgNP spots on the hydrophobic filter paper with the different number of CNF coatings.

2. 3. Reproducibility of CNF coated filter paper-based SERS sensors

To compare the reproducibility of hydrophobic filter paper-based SERS sensors treated with the different number of CNF coatings, the SERS spectrum of each sensor was measured. Each sensor was treated with 5 μL of 1 μM R6G solution. The SERS spectrum of each sensor was averaged 15 different AgNP spots on each sensor using 40x objective lens. The spot-to-spot variation of SERS intensity was quantified by the 7 different bands of R6G. The SERS spectra, SERS intensity and RSD of SERS intensity of each R6G band were shown in Figure 2-8 and Table 2-1. As the number of CNF coatings on the hydrohpobic filter paper was increased, the SERS intensity was gradually increased and highest when double CNF coatings was introduced on the hydrophobic filter paper. In addition, the RSD of each SERS band of R6G was dramatically decreased up to 9% when double CNF coating introduced on hydrophobic filter paper. These results suggested that a simple CNF coating on filter paper surface could greatly improved the uniformity of the AgNP distribution on filter paper, which induced increase of the reproducibility of paper-based SERS sensors.

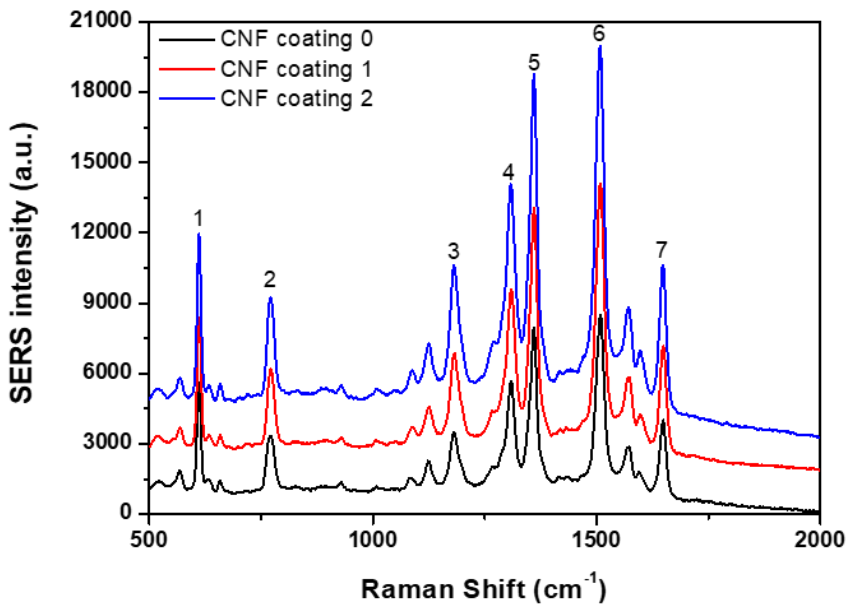

Figure 2-8. The SERS spectra of R6G on AgNP spots on each CNF coated hydrophobic filter paper-based SERS sensor treated with the different number of CNF coatings. The number on SERS spectra meant R6G bands for comparing RSDs of CNF coated hydrophobic filter paper-based SERS sensors.

	CNF coating : 0		CNF coating : 1		CNF coating : 2	
Band No.	Intensity (a.u.)	RSD (%)	Intensity (a.u.)	RSD (%)	Intensity (a.u.)	RSD (%)
1	5118	28.5	6028	17.4	6842	9.3
2	2677	28.3	3508	17.2	4062	8.6
3	2537	28.8	3965	16.6	4650	9.0
4	4618	28.6	6416	15.9	7433	8.5
5	6911	28.7	10747	15.9	12528	8.7
6	7523	29.5	11488	15.4	13319	8.0
7	3442	29.2	5213	16.0	6054	9.3

Table 2-1. The SERS intensities and RSDs of each R6G band of each CNF coated hydrophobic filter paper-based SERS sensor treated with the different number of CNF coatings.

2. 4. Sensitivity test of CNF coated paper-based SERS sensors

To compare the sensitivity of the filter paper-based SERS sensors depending on number of CNF coatings, the SERS spectra of sensor treated with 5 μL of 1 μM 4-ATP solutions with different concentrations from 0.1 nM to 1000 nM were measured as shown in Figure 2-9. The SERS spectra were obtained from 15 different AgNP spots on each sensor using 40x objective lens. The SERS intensities of the 1073 cm^{-1} band of 4-ATP of different concentrations were shown in Figure 2-10. The SERS intensities of filter paper-based SERS sensors treated by CNF coating were increased more than 2 times compared with that of CNF untreated filter paper-based SERS sensor. Furthermore, the LODs of 4-ATP of filter paper-based was decreased as the number of CNF coatings was increased, and the that of double CNF coating introduced filter paper-based SERS sensor was decreased up to 0.426 nM as shown in Table 2-2. These results indicated that the inroducing CNF coating on paper-based SERS sensor improved uniformity of surface of filter paper, which was affected to sensitivity of paper-based SERS sensor.

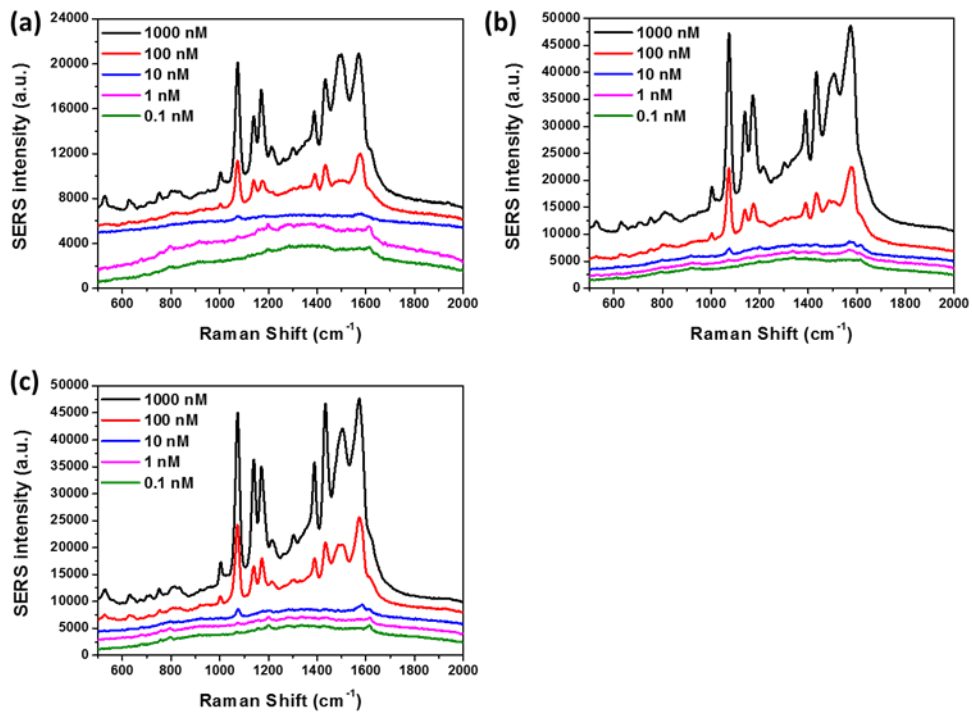

Figure 2-9. The SERS spectra of AgNP spots on each CNF coated hydrophobic filter paper-based SERS sensor treated with different concentrations of 4-ATP. The filter paper-based SERS sensor was treated with the different number of CNF coatings. The SERS spectra of (a) CNF untreated filter paper-based SERS sensor, (b) one CNF coating on filter paper-based SERS sensor and (c) double CNF coatings on filter paper-based SERS sensor.

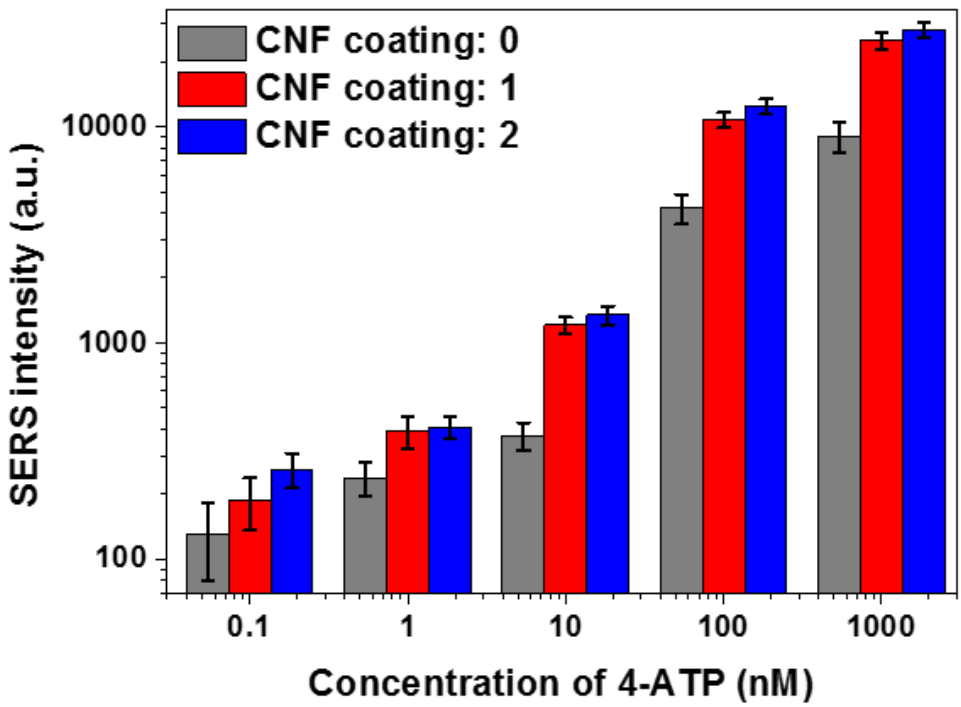

Figure 2-10. The averaged SERS intensities of 1073 cm^{-1} band of 4-ATP treated on AgNP spots on each CNF coated hydrophobic filter paper-based SERS sensor. The concentrations of 4-ATP were varied from 0.1 nM to 1000 nM.

Sample	a (intercept of fitted line)	b (slope of fitted line)	σ (Standard deviation of SERS intensity of blank sample)	y_0 (SERS intensity of blank sample)	R^2	LOD (nM)
CNF: 0	2.320	0.502	70.061	197.36	0.904	3.782
CNF: 1	2.829	0.557	173.737	385.94	0.925	1.702
CNF: 2	2.946	0.513	67.790	366.88	0.928	0.426

Table 2-2. Estimation of limit of detections (LODs) of 4-ATP of each filter paper-based SERS sensor with the different number of CNF coatings.

Chapter III. Expanding generality of SERS based molecular detection by charge-selective paper-based SERS sensor

1. Experimental

1. 1. Chemicals and reagents

Silver nitrate ($AgNO_3$, 99.999 %), sodium citrate tribasic dehydrate ($C_6H_5O_7Na_3 \cdot 2H_2O$, 99 %), rhodamine 6G (R6G, $C_{28}H_{31}N_2O_3Cl$, 99 %), sunset yellow (SY, $C_{16}H_{10}N_2Na_2O_7S_2$, 90 %), methyl orange (MO, $C_{14}H_{14}N_3NaO_3S$, 85 %), aniline (AN, $C_6H_5NH_2$, 99.5 %), benzoic acid (BA, C_6H_5COOH, 99.5 %), 4-methylaniline (4-MA, $CH_3C_6H_4NH_2$, 99 %), 4-methylbenzoic acid (4-MB, $CH_3C_6H_4COOH$, 98 %), hydrochloric acid (HCl, 37%), sodium hydroxide (NaOH, 98%), sodium chloride (NaCl, 99%) and poly(diallyldimethylammonium chloride) (PDDA, $(C_8H_{16}ClN)_n$, 35 wt% in H_2O, average molecular weight < 100,000) were purchased from Sigma-Aldrich (St. Louis, MO, USA). Tris(2,2'-bipyridyl)ruthenium(II) chloride hexahydrate ($Ru(bpy)_3$, $C_{30}H_{24}Cl_2N_6Ru \cdot 6H_2O$, 98 %) was purchased from Tokyo chemical industry Co., LTD. (Tokyo, Japan). Filter paper was purchased from Advantec (grade 5C, Dublin, CA, USA) and alkyl ketene dimer (AKD) was purchased from Solenis (Hercon-WI 155, Kimchun, Korea). Carboxymethyl cellulose (CMC) was purchased from CP Kelco Korea (DS 0.78, Finnfix 5, CP Kelco Korea). A bleached eucalyptus kraft pulp was purchased from Moorin P&P (Seoul, Korea). All chemicals and materials were used without further purification.

1. 2. Preparation of positive charged polymer encapsulated AgNPs

To change the surface charge of citrated-based AgNP from negative to positive, the AgNP was encapsulated by PDDA polymer[100]. To encapsulate the AgNP by PDDA polymer, the 20 mL of AgNP solution was centrifugation with the condition of 3000 rpm and 15 min for removing excess citrate in AgNP solution. After removing of excess citrate, the centrifugated AgNP was dispersed in 20 mL of DW, and the AgNP solution of 20 mL was dispersed in 20 mL of PDDA solution (0.5 vol%, in DW) for encapsulation PDDA polymer to the AgNP surface. The mixed solution was vigorous stirred about 3 h. After stirring, the mixed solution was centrifuged with the condition of 3000 rpm, 15 min, twice. After centrifugation, the PDDA encapulated AgNP solution was dispersed in 2 mL of DW.

1. 3. Fabrication of SERS-active AgNP and AgNP@PDDA spots on modified filter paper

To fabricate charge-selective paper-based SERS sensor, the AgNP and PDDA encapsulated AgNP (AgNP@PDDA) were used to fabricate SERS-active spots on filter paper surface. The filter paper was used as previously developed filter paper, which treated by AKD and double CNF coating for increasing hydrophobicity and uniformity of filter paper. On the CNF coated hydrophobic filter paper, the 3 μL of AgNP and AgNP@PDDA solutions were dropped and dried to fabricate AgNP and AgNP@PDDA spots, and then, 2 μL droplets of analyte solution were dropped and dried on the AgNP and AgNP@PDDA spots for SERS measurement. The FE-SEM

images and photographs of AgNP and AgNP@PDDA spots on the filter paper were shown in Figure 3-1 and Figure 3-2.

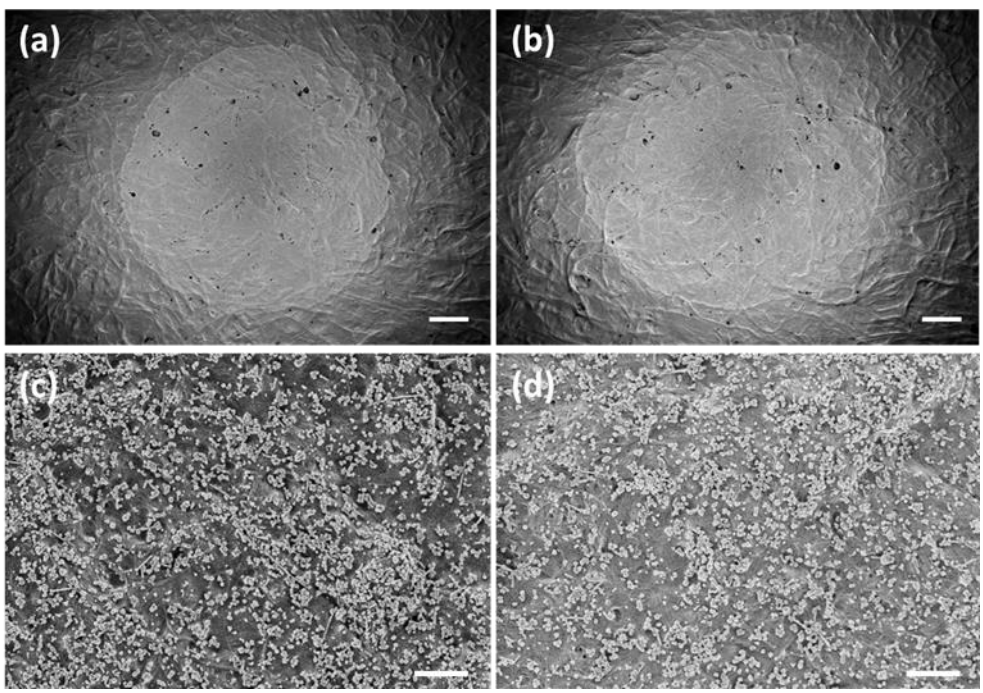

Figure 3-1. The AgNP and AgNP@PDDA distributions on CNF coated hydrophobic filter paper. The low magnified FE-SEM images of (a) AgNP and (b) AgNP@PDDA spots, and the high magnified FE-SEM images of (c) AgNP and (d) AgNP@PDDA spots. The scale bars of (a), (b) were 100 μm, and those of (c), (d) were 1 μm.

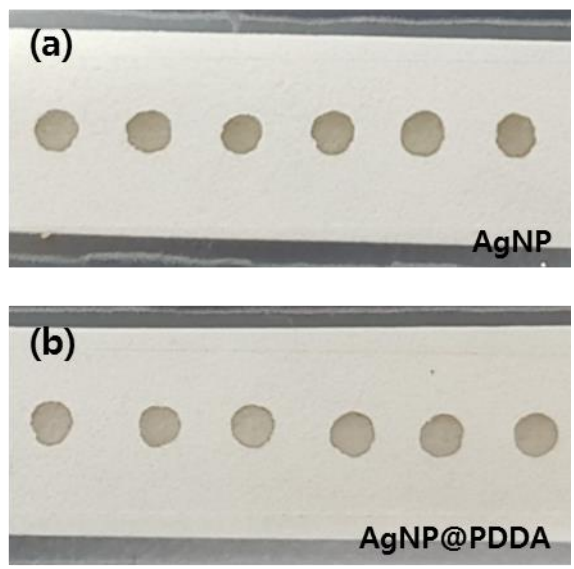

Figure 3-2. The Photographs of charge-selective paper-based SERS sensor. (a) AgNP and (b) AgNP@PDDA spots on filter paper.

1. 4. Samples preparation for SERS measurement

To verify the feasibility of charge-selective SERS detection of charge-selective paper-based SERS sensor, R6G, $Ru(bpy)_3$, MO, SY, AN, BA, 4-MA, 4-MB were used as test analytes. R6G, $Ru(bpy)_3$, MO and SY were dissolved in DW. AN and 4-MA were dissolved in a solution of 10 mM HCl, and BA and 4-MB were dissolved in a solution of 10 mM NaOH for fully ionization of each analyte. The structures of analytes were shown in Figure 3-3.

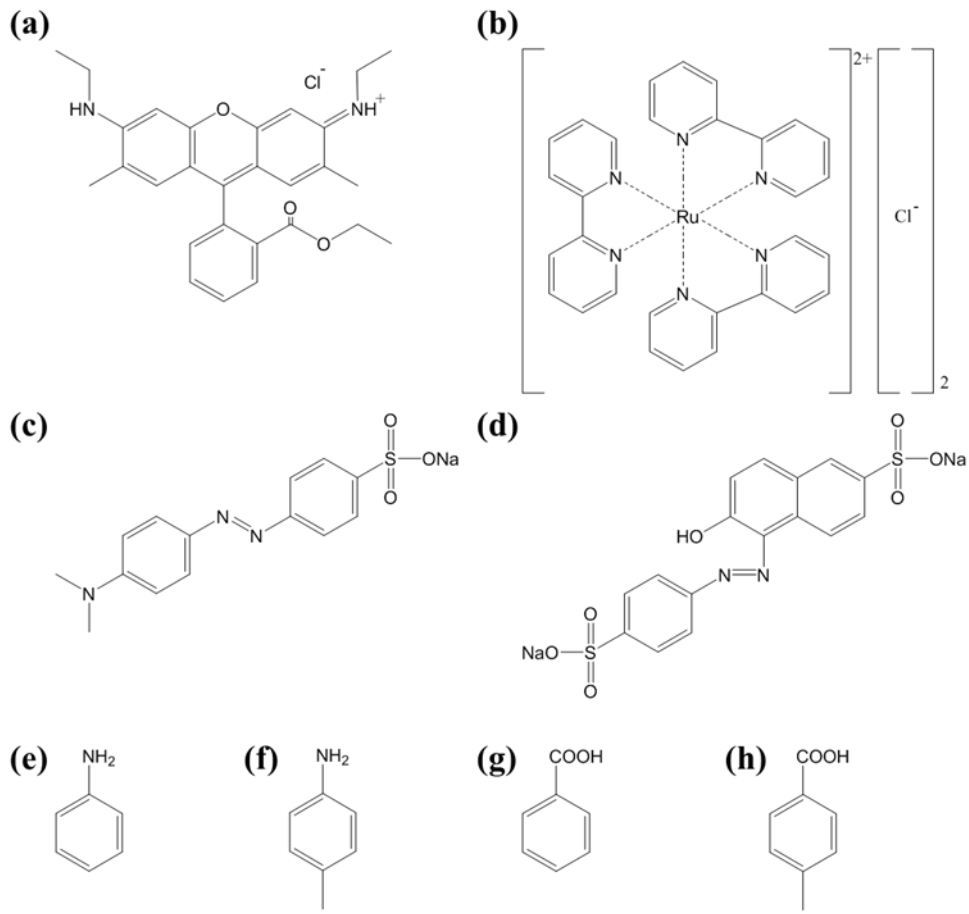

Figure 3-3. The structures of analytes. (a) Rhodamine 6G (R6G), (b) tris(2,2'-bipyridyl)ruthenium(II) chloride hexahydrate ($Ru(bpy)_3$), (c) methyl orange (MO), (d) sunset yellow (SY), (e) aniline (AN), (f) 4-methylaniline (4-MA), (g) benzoic acid (BA) and (h) 4-methylbenzoic acid (4-MB).

1. 5. SERS measurement

The SERS spectra were obtained by a hand-made large-area scanning system combined with micro Raman system. The laser line was used 643-nm laser (110-81040-019, Ondax, US) for excitation source, and the sample power of laser was set as 1.0 mW. The objective lens was used 20x of magnification (NA=0.40, Olympuse, Japan), and the scanning area was 600 μm × 600 μm. The acquisition time was 40 sec.

2. Results and Discussion

2. 1. Design of charge-selective paper-based SERS sensor

Generally, the SERS intensity was enhacned when the molecule was closed to the surface of nanoparticles. However, due to the affinity difference between molecule and nanoparticle by functional groups in molecule, only a few molecules, (e.g., those containing thiol (-SH) and isocyanide (-NC) functional groups), were used for SERS detection[32-33]. By the reason, to expand the generality of SERS based molecular detection, a charge-selective paper-based SERS sensor was developed for detecting the polar molecules by electrostatic attraction force. Two different surface charged AgNPs were used to detect the polar molecules by electrostatic attraction between polar molecule and AgNPs in this study. The surface modification of AgNP was shown in Figure 3-4. The citrated-based AgNP have a negative surface charge because the AgNP was capped by citrate ions presented in a trivalent anion state in solution. Using AgNP, positively charged molecules could be detected by electrostatic attraction between the molecules and nanoparticles, however, the AgNPs did not provide effective detection of negatively charged molecules because of electrostatic repulsion between the AgNP and negatively charged molecules. Thus, the surface charge of the AgNP was changed from negative to positive by encapsulation of positively charged PDDA polymer on AgNP (AgNP@PDDA) to detect negatively charged molecules. The overall fabrication scheme of charge-selective paper-based SERS sensors using AgNP and AgNP@PDDA is shown in Figure 3-5.

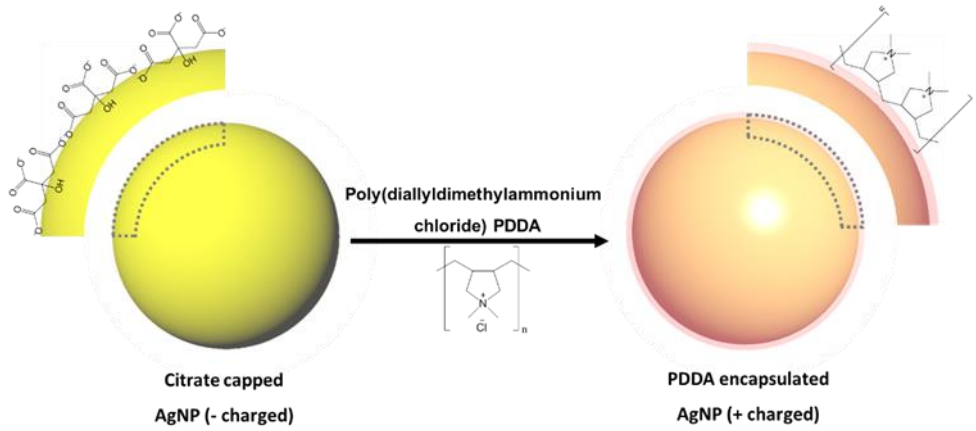

Figure 3-4. The illustration of surface modification of AgNP by PDDA polymer for charge-selective paper-based SERS sensor.

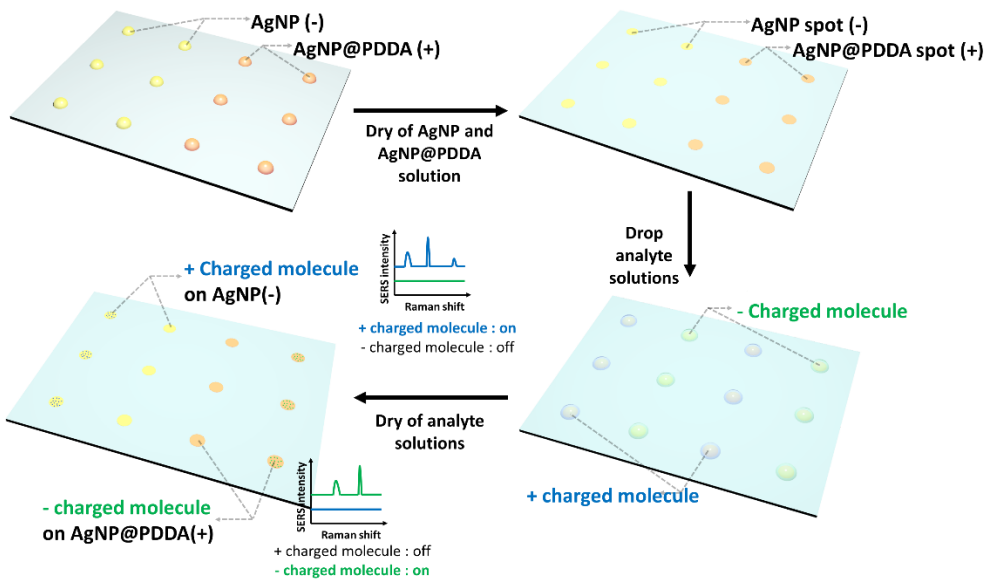

Figure 3-5. The schematic illustration of fabrication of charge-selective paper-based SERS sensor.

2. 2. Characterization of surface modification of AgNP and AgNP@PDDA

To verify the surface modification of AgNP by PDDA, the zeta-potential, UV/Vis spectrum, and HR-TEM images of the AgNP and AgNP@PDDA were measured as shown in Figure 3-6. The AgNP and AgNP@PDDA showed a plasmonic band at 410 nm and 422 nm, respectively. The encapsulation of AgNP by PDDA resulted in a red shift of the plasmonic band of AgNP because the refractive index of the AgNP increased by polymer encapsulation[101-102]. Furthermore, the zeta-potential of the AgNP changed from negative to positive after PDDA polymer encapsulation of the AgNP. The zeta-potentials of AgNP and AgNP@PDDA were -21.5 and 30.5 mV, respectively. The HR-TEM images directly showed that the AgNP@PDDA were encapsulated by PDDA. Before modification of the AgNP, no shell was existed on the AgNP as shown in Figure 3-6c. However, after surface modification, a 2-3 nm shell on the AgNP was seen as shown in Figure 3-6d. These results confirmed that the polymer successfully encapsulated the AgNP and changed the surface charge of the AgNP from negative to positive.

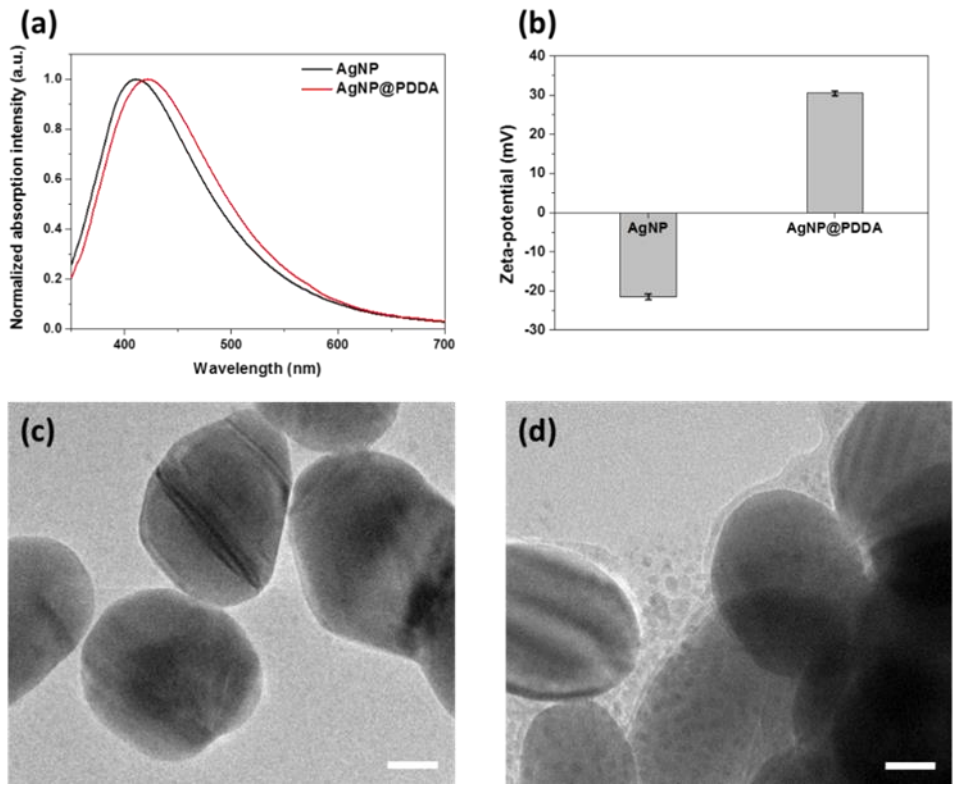

Figure 3-6. Characterization of AgNP and AgNP@PDDA. (a) The UV/Vis spectrum, (b) the zeta-potentials of AgNP and AgNP@PDDA, the HR-TEM image of (c) AgNP and (d) AgNP@PDDA. Inset scale bar was represented 20 nm.

To confirm the activation of the charge-selective paper-based SERS sensor with different pH values, the zeta-potentials of AgNP and AgNP@PDDA were measured in deionized water, 10 mM HCl, and NaOH solutions, which were the same conditions with analyte preparation for the SERS measurements. As shown in Figure 3-7, the zeta-potentials of the AgNP and AgNP@PDDA did not significantly changes with the different pH solution. Regardless of the pH of the solutions, the zeta-potentials of AgNP remained between -40 and -20 mV, and those of AgNP@PDDA remained between 20 and 30 mV. These results confirm that the pH value of solution did not significantly affect the surface charges of the AgNP and AgNP@PDDA.

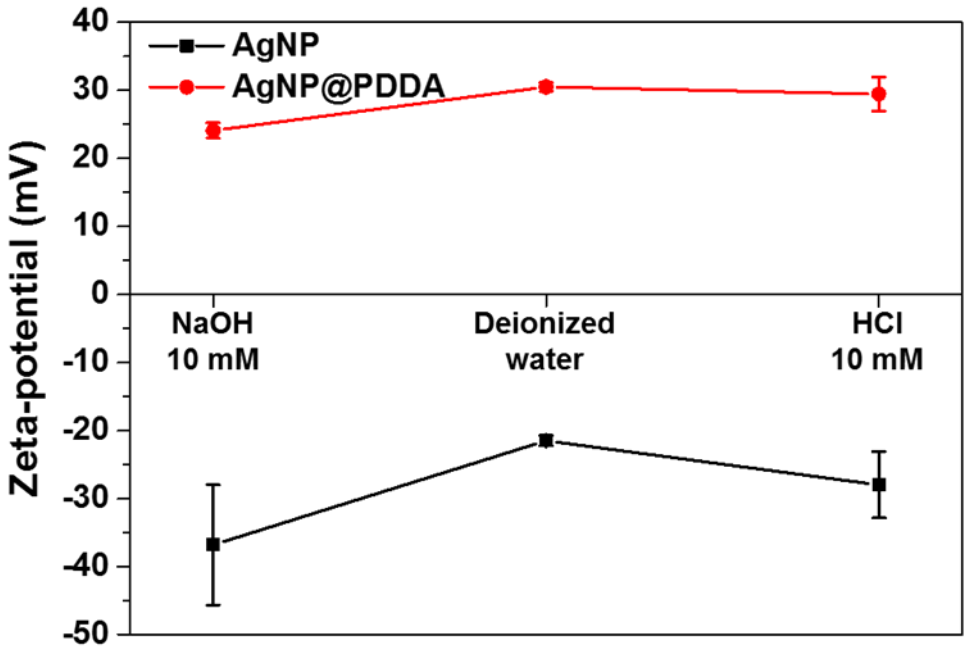

Figure 3-7. The zeta-potentials of AgNP and AgNP@PDDA with different pH value of solutions.

2. 3. Evaluation of charge-selective paper-based SERS sensor using charged Raman dyes

To evaluate the feasibility of the charge-selective paper-based SERS sensor, charged Raman dyes were applied to the developed charge-selective paper-based SERS sensor. R6G and $Ru(bpy)_3$ were used as the positively charged Raman dyes, and MO and SY were used as the negatively charged Raman dyes. The concentrations of R6G, $Ru(bpy)_3$, MO, and SY were 0.1, 1, 10, and 10 μM, respectively. The SERS spectra of the AgNP and AgNP@PDDA spots treated with each analyte were shown in Figure 3-8. The SERS signals of the positively charged molecules were significantly enhanced at the AgNP spots, however, the SERS signals of the negatively charged molecules were almost absent. The SERS signal of each analyte at the AgNP@PDDA spots show an opposite tendency. The SERS signals of the negatively charged molecules were significantly enhanced at the AgNP@PDDA spots. The different phenomena originate from the different capping agents of AgNP and AgNP@PDDA. The surface charge of the AgNP was negative because of the negative charge of citrate ion, which causes an electrostatic attraction with positively charged molecules, such as R6G and $Ru(bpy)_3$. However, the AgNP electrostatically repulsed with the negatively charged Raman dyes, such as MO and SY. As a result, the negatively charged molecules moved away from the surface of the AgNP, and the SERS signals were reduced on the AgNP spots. However, the opposite results were obtained for AgNP@PDDA, which exhibited positive surface charge. The SERS signals of MO and SY, which was negative charged Raman dyes, were

enhanced, however, the SERS signals of R6G and $Ru(bpy)_3$ were reduced. These results indicate that the paper-based SERS sensors by using AgNP and AgNP@PDDA were suitable for charge-selective SERS detection by electrostatic attraction and repulsion force between polar molecule and nanoparticle.

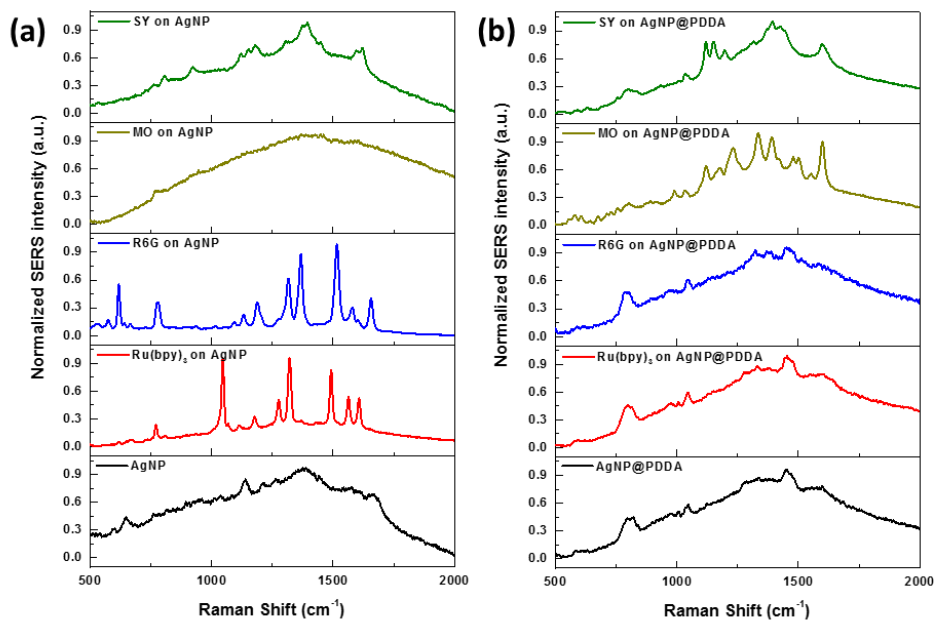

Figure 3-8. The feasibility test of charge-selective paper-based SERS sensor by charged Raman dyes. (a) The SERS spectra of charged Raman dyes on AgNP spots and (b) the SERS spectra of charged Raman dyes on AgNP@PDDA spots.

2. 4. Effect of ionization of aniline and benzoic acid on SERS intensity

To apply the charge-selective paper-based SERS sensor to detect polar organic pollutants, AN and BA derivatives were treated on the charge-selective paper-based SERS sensor. The AN derivatives were ionized and show a positive charge in DW because of the amine functional group in the AN derivatives. Likewise, the BA derivatives were ionized and show a negative charge in DW because of the carboxylic acid functional group in the BA derivatives. However, the most of the AN and BA was existed in an un-ionized state in DW because of the low dissociation constant of AN and BA derivatives. Thus, it is hard to detect AN and BA derivatives using charge-selective SERS detection. To identify the effect of ionization of polar organic pollutants about the SERS intensity on charge-selective paper-based SERS sensor, AN and BA were treated on paper-based SERS sensors with different sample preparations. For SERS measurements, a 10 mM AN solution was prepared in DW and 10 mM HCl, and a 10 mM BA solution was prepared in DW and 10 mM NaOH. The AN solutions were treated on the AgNP spots, and the BA solutions were treated on the AgNP@PDDA spots. The SERS spectrum of each analyte was shown in Figure 3-9. The SERS intensities of AN and BA dissolved in DW showed low SERS signals, however, AN dissolved in HCl and BA dissolved in NaOH showed more enhanced SERS intensities than those of AN and BA dissolved in DW. These phenomena implied that ionization of polar organic pollutants affected the SERS intensity. AN and BA were non-ionized in deionized water (i.e., most were neutral

molecules) because of low dissociation constants, the most of AN and BA were not electrostatically attracted with the AgNPs and AgNP@PDDA, showed low SERS signals. However, the most of the AN dissolved in the HCl solution was protonated by HCl, and the protonated AN showed positive charge. Furthermore, the most of the BA dissolved in the NaOH solution was deprotonated by NaOH, and the deprotonated BA had negative charge. The ionized AN and BA were electrostatically attracted with the AgNP and AgNP@PDDA and showed enhanced SERS signals compared to those of un-ionized AN and BA in DW. Therefore, charge-selective SERS detection was more effective when the polar organic pollutants were dissolved in acidic or basic solutions to increase their ionization.

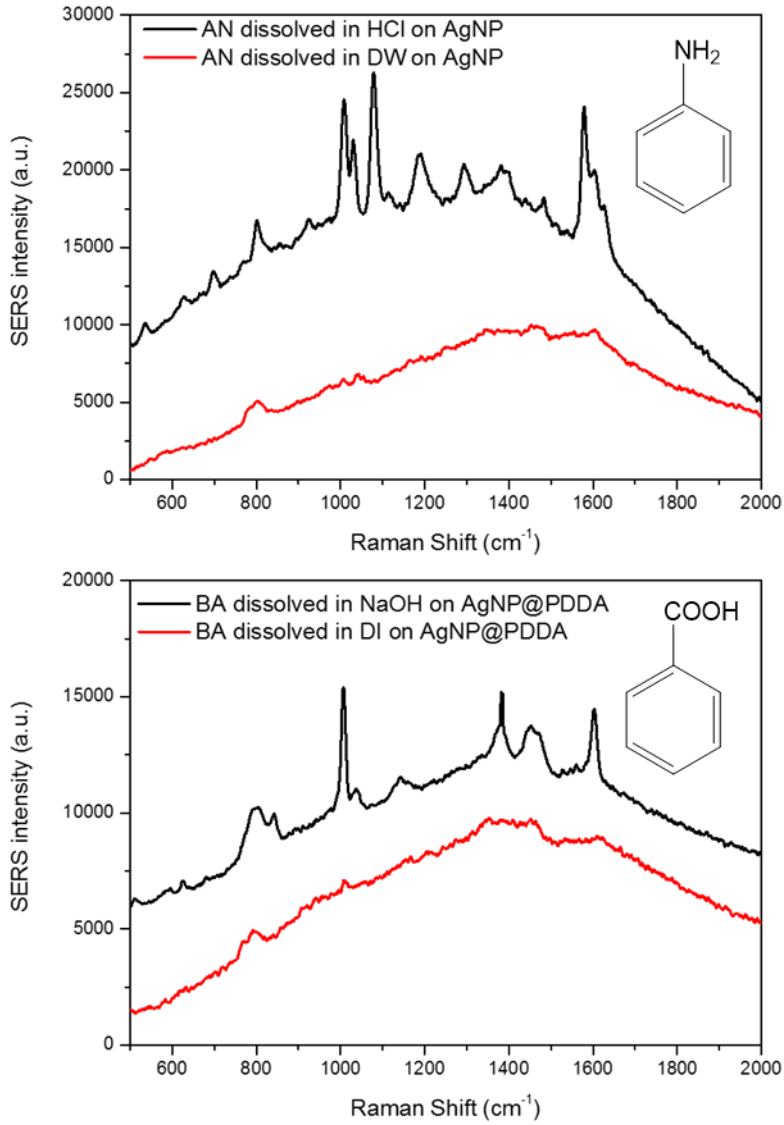

Figure 3-9. Ionization dependency of SERS intensities of polar organic pollutants. The SERS spectra of 10 mM of (a) AN on AgNP spot and (b) BA on AgNP@PDDA spot dissolved with different conditions of sample preparations.

2. 5. Application to detect polar organic pollutants by charge-selective paper-based SERS sensor

To apply the charge-selective paper-based SERS sensor, AN, 4-MA, BA and 4-MB were used as polar organic pollutants to the charge-selective paper-based SERS sensor. For ionization of polar organic pollutants, AN and 4-MA were dissolved in 10 mM HCl, and BA and 4-MB were dissolved in 10 mM NaOH. The analyte solutions were treated on the charge-selective paper-based SERS sensor, and the SERS spectrum of each analyte was shown in Figure 3-10. Figure 3-10a and 3-10b showed that AN and 4-MA showed more enhanced SERS signals on the AgNP spot than those on the AgNP@PDDA spot. On the contrary, BA and 4-MB showed more enhanced SERS signals on the AgNP@PDDA spot than those on the AgNP spot, as shown in Figure 3-10c and 3-10d. Protonated AN and 4-MA were electrostatically attracted by the negative charge of the AgNP, and deprotonated BA and 4-MB were electrostatically attracted by the positive charge of AgNP@PDDA. Therefore, the charge-selective paper-based SERS sensor was suitable for detecting polar organic pollutants.

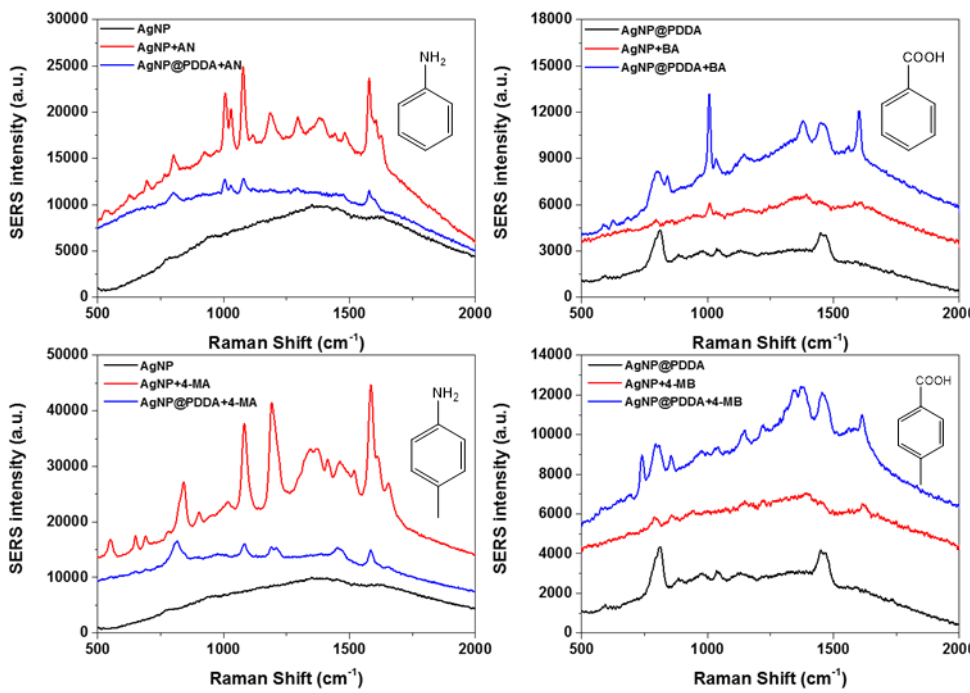

Figure 3-10. The feasibility test of polar organic pollutant to charge-selective paper-based SERS sensor. The SERS spectra of 10 mM of (a) AN, (b) 4-MA, (c) BA and (d) 4-MB on the charge-selective paper-based SERS sensor.

To evaluate the sensitivity of charge-selective paper-based SERS sensor, AN and BA were used as polar organic pollutants. Each analyte was treated with sample conditions in previous test. The concentration of analytes were varied from 0 to 10000 μM. The SERS spectra of analytes with different concentrations were shown in Figure 3-11. To compare the SERS intensites of AN and BA, the 1010 cm^{-1} band of AN and BA were averaged from 7 different AgNP and AgNP@PDDA spot on the charge-selective paper-based SERS sensors treated with different concentrations of analyte. The averaged SERS intensities of AN and BA were shown in Figure 3-12. Both two analytes were detected at the level of tens of micromolar concentration with less than 10 % of RSDs. From these results, the charge-selective paper-based SERS sensor were adequate for detecting polar organic pollutants with high sensitivity and reproducibility. In addition, by applying charge-selective SERS detection in paper-based SERS sensor, it was shown the possibility of expanding generality of SERS based molecular detection by electrostatic attraction between molecules and nanoparticles.

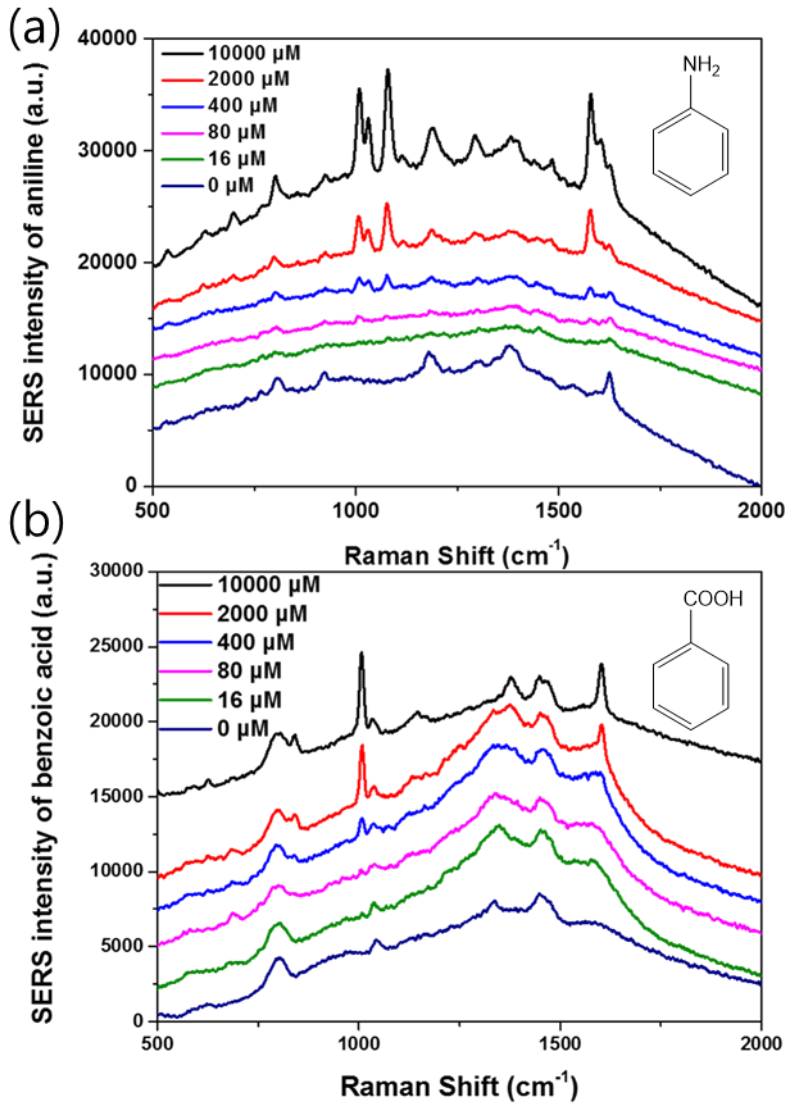

Figure 3-11. The sensitivity test of charge-selective paper-based SERS sensor by using polar organic pollutants. The SERS spectra of (a) AgNP spots treated with different concentrations of AN and (b) AgNP@PDDA spots treated with different concentrations of BA.

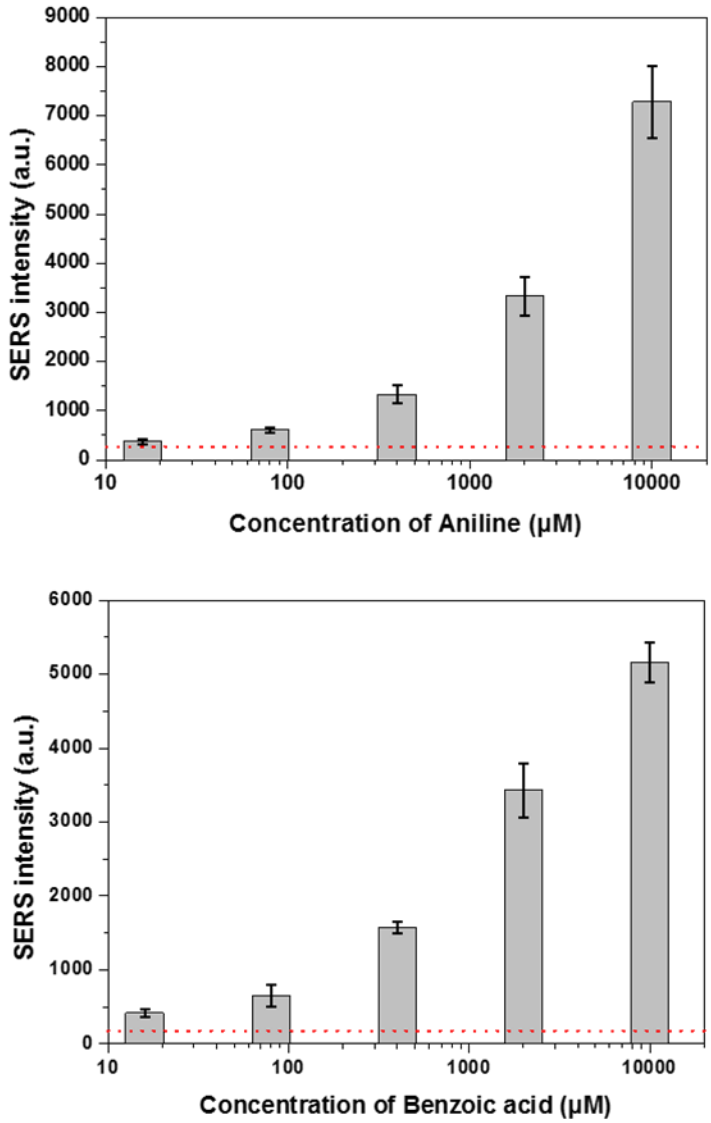

Figure 3-12. The SERS intensites of (a) 1010 cm^{-1} band of AN and (b) BA with different concentrations of AN and BA. The dotted redline means SERS intensity of blank sample (= 0 μM).

Conclusion

In summary, we demonstrated a highly sensitive and reproducible filter paper-based SERS sensor with hydrophobic surface provided by AKD treatment and highly uniform paper surface from CNF coating. In addition, charge-selective paper-based SERS sensor was developed by using surface modified AgNPs to detect polar organic pollutants by electrostatic attraction between polar pollutant and nanoparticle for expanding generality of SERS based molecular detection.

To increase the sensitivity and reproducibility of filter paper-based SERS sensor, at first, hydrophobic filter paper-based SERS sensor was fabricated by treatment with AKD on filter paper. By using the hydrophobic filter paper, the AgNP and analyte solutions were prevented from absorption into the filter paper and were retained on the surface of filter paper until drying. Unlike the conventional filter paper-based SERS sensors, the hydrophobic filter paper-based SERS sensor was found to form numerous SERS hot-spots composed of AgNP clusters on the surface of filter paper, without absorption of AgNP into the filter paper. Furthermore, the concentration of AgNP solution treated on the surface of filter paper to form AgNP spot was optimized for highly sensitive and reproducible SERS intensity. The hydrophobic filter paper-based SERS sensor showed highly sensitive and reproducible SERS detection of pesticides at the sub-nanomolar level with 6 % of RSD.

Second, the uniformity of the surface of the hydrophobic filter paper-based SERS sensor was increased by introducing CNF coatings for highly reproducible SERS

detection. To increase the sensitivity of SERS sensor, SERS spectra were measured using a objective lens with high value of NA. However, conventional paper-based SERS sensors showed low reproducibility of the SERS signal when objective lens with high value of NA was used to apply SERS measurement because of decreasing of confocal volume. Conventional paper-based SERS sensors showed non-uniform surface by high surface roughness and numerous pores on the paper surface which were originated by variation of size and conformation of the cellulose fibrils in the paper, resulted in low reproducibiltiy. To overcome disadvantage of paper-based SERS sensor, the CNF coating was introduced on hydrophobic filter paper. By introducing CNF coating, the uniformity of the surface of filter paper was increased because the CNF filled the pores and reduced surface roughness of the filter paper, resulted in increasing reproducibility of filter paper-based SERS sensor. As a result, the AgNP coverage of hydrophobic filter paper treated with double CNF coatings were increased up from 87% to 95%, and the AgNP distribution on the CNF coated hydrophobic filter paper-based SERS sensor were more uniform than that of the CNF untreated hydrophobic filter paper. As the number of CNF coatings on the hydrophobic filter paper increased, the RSDs of the SERS intensities of hydrophobic filter paper were decreased from 28% to 9%, and the LODs of the paper-based SERS sensors were decreased from 3.782 to 0.426 nM by introducing CNF coatings on hydrophobic filter paper.

Finally, charge-selective paper-based SERS sensor was developed to expand the generality of SERS based molecular detection. Due to the affinity difference between the molecule and metal depending on functional group of molecules, only a few molecules, which have specific functional group such as thiol and isocyanide, could be detected by conventional SERS sensors, resulted in lack of generality of SERS based molecular detection. To expand generality of SERS based molecular detection, charge-selective SERS detection was applied to paper-based SERS sensor. To acheive charge-selective SERS detection, charge-selective paper-based SERS sensor was fabricated using negatively charged AgNP and positively charged AgNP@PDDA to detect counter-charged molecules.AgNP was encapsulated by PDDA polymer which was positive charged polymer to synthesize positively charged AgNP@PDDA, and AgNP and AgNP@PDDA was applied to the surface of CNF coated hydrophobic filter paper. The surface modification of AgNP was confirmed by changing of UV/Vis spectrum, zeta-potential and HR-TEM images. To verify the feasibility of the carge-selective paper-based SERS sensor, charged Raman dyes such as R6G, $Ru(bpy)_3$, MO, and SY were applied to charge-selective paper-based SERS sensor. The positively charged Raman dyes such as R6G and $Ru(bpy)_3$ were detected on AgNP spot, and the negatively charged Raman dyes such as MO and SY were detected on AgNP@PDDA spot by electrostatic attraction. It was confirmed that a charge-selective SERS detection was well operated by charge-

selective paper-based SERS sensor. Finally, the charge-selective paper-based SERS sensor was applied to detect polar organic pollutants, such as aniline and benzoic acid derivatives. Aniline and benzoic acid were detected at the level of tens of micromolar concentration with highly reproducible detection, which was showed about 10% of RSD.

The presented paper-based SERS sensor indicated that hydrophobic modification and CNF coating on filter paper increased the sensitivity and reproducibility of paper-based SERS sensors without using complicated and expensive processes. Furthermore, the developed paper-based SERS sensor could detect molecules, which could not detected by using conventional paper-based SERS sensors by applying charge-selective detection to the paper-based SERS sensor. The charge-selective detection of paper-based SERS sensor extended the detection generality of SERS. The presented paper-based SERS sensor could be as a guidance in the field of SERS-based detection to develop universal paper-based SERS sensors in the future.

References

1. Raman, C. V.; Krishnan, K. S., A new type of secondary radiation. *Nature* **1928,** *121*, 501-502.

2. Zhu, X.; Xu, T.; Lin, Q.; Duan, Y., Technical Development of Raman Spectroscopy: From Instrumental to Advanced Combined Technologies. *Applied Spectroscopy Reviews* **2014,** *49* (1), 64-82.

3. Moskovits, M., Surface-enhanced spectroscopy. *Reviews of Modern Physics* **1985,** *57* (3), 783-826.

4. Fleischmann, M.; Hendra, P. J.; McQuillan, A. J., Raman spectra of pyridine adsorbed at a silver electrode. *Chemical Physics Letters* **1974,** *26* (2), 163-166.

5. Campion, A.; Kambhampati, P., Surface-enhanced Raman scattering. *Chemical Society Reviews* **1998,** *27* (4), 241-250.

6. Le Ru, E. C.; Blackie, E.; Meyer, M.; Etchegoin, P. G., Surface Enhanced Raman Scattering Enhancement Factors: A Comprehensive Study. *The Journal of Physical Chemistry C* **2007,** *111* (37), 13794-13803.

7. Ding, S.-Y.; You, E.-M.; Tian, Z.-Q.; Moskovits, M., Electromagnetic theories of surface-enhanced Raman spectroscopy. *Chemical Society Reviews* **2017,** *46* (13), 4042-4076.

8. Schatz, G. C.; Young, M. A.; Van Duyne, R. P., Electromagnetic mechanism of SERS. *Surface-Enhanced Raman Scattering: Physics and Applications* **2006,** *103*, 19-45.

9. Jun, B. H.; Kim, G.; Noh, M. S.; Kang, H.; Kim, Y. K.; Cho, M. H.; Jeong, D. H.; Lee, Y. S., Surface-enhanced Raman scattering-active nanostructures and strategies for bioassays. *Nanomedicine* **2011,** *6* (8), 1463-1480.

10. Chang, H.; Kang, H.; Ko, E.; Jun, B.-H.; Lee, H.-Y.; Lee, Y.-S.; Jeong, D. H., PSA Detection with Femtomolar Sensitivity and a Broad Dynamic Range Using SERS Nanoprobes and an Area-Scanning Method. *ACS Sensors* **2016,** *1* (6), 645-649.

11. Mohs, A. M.; Mancini, M. C.; Singhal, S.; Provenzale, J. M.; Leyland-Jones, B.; Wang, M. D.; Nie, S., Hand-held Spectroscopic Device for In Vivo and Intraoperative Tumor Detection: Contrast Enhancement, Detection Sensitivity, and Tissue Penetration. *Analytical Chemistry* **2010,** *82* (21), 9058-9065.

12. Sha, M. Y.; Xu, H.; Natan, M. J.; Cromer, R., Surface-Enhanced Raman Scattering Tags for Rapid and Homogeneous Detection of Circulating Tumor Cells in the Presence of Human Whole Blood. *Journal of the American Chemical Society* **2008,** *130* (51), 17214-17215.

13. Craig, A. P.; Franca, A. S.; Irudayaraj, J., Surface-Enhanced Raman Spectroscopy Applied to Food Safety. In *Annual Review of Food Science and*

Technology, Vol 4, Doyle, M. P.; Klaenhammer, T. R., Eds. Annual Reviews: Palo Alto, 2013; Vol. 4, pp 369-380.

14. Radu, A. I.; Kuellmer, M.; Giese, B.; Huebner, U.; Weber, K.; Cialla-May, D.; Popp, J., Surface-enhanced Raman spectroscopy (SERS) in food analytics: Detection of vitamins B2 and B12 in cereals. *Talanta* **2016,** *160*, 289-297.

15. Demeritte, T.; Kanchanapally, R.; Fan, Z.; Singh, A. K.; Senapati, D.; Dubey, M.; Zakar, E.; Ray, P. C., Highly efficient SERS substrate for direct detection of explosive TNT using popcorn-shaped gold nanoparticle-functionalized SWCNT hybrid. *Analyst* **2012,** *137* (21), 5041-5045.

16. Shafer-Peltier, K. E.; Haynes, C. L.; Glucksberg, M. R.; Van Duyne, R. P., Toward a Glucose Biosensor Based on Surface-Enhanced Raman Scattering. *Journal of the American Chemical Society* **2003,** *125* (2), 588-593.

17. Pozzi, F.; Leona, M., Surface-enhanced Raman spectroscopy in art and archaeology. *Journal of Raman Spectroscopy* **2016,** *47* (1), 67-77.

18. Kang, J. W.; So, P. T. C.; Dasari, R. R.; Lim, D.-K., High Resolution Live Cell Raman Imaging Using Subcellular Organelle-Targeting SERS-Sensitive Gold Nanoparticles with Highly Narrow Intra-Nanogap. *Nano Letters* **2015,** *15* (3), 1766-1772.

19. Huefner, A.; Kuan, W.-L.; Barker, R. A.; Mahajan, S., Intracellular SERS Nanoprobes For Distinction Of Different Neuronal Cell Types. *Nano Letters* **2013,**

13 (6), 2463-2470.

20. Lahr, R. H.; Vikesland, P. J., Surface-Enhanced Raman Spectroscopy (SERS) Cellular Imaging of Intracellulary Biosynthesized Gold Nanoparticles. *ACS Sustainable Chemistry & Engineering* **2014,** *2* (7), 1599-1608.

21. Wei, H.; Hossein Abtahi, S. M.; Vikesland, P. J., Plasmonic colorimetric and SERS sensors for environmental analysis. *Environmental Science: Nano* **2015,** *2* (2), 120-135.

22. Patze, S.; Huebner, U.; Liebold, F.; Weber, K.; Cialla-May, D.; Popp, J., SERS as an analytical tool in environmental science: The detection of sulfamethoxazole in the nanomolar range by applying a microfluidic cartridge setup. *Analytica Chimica Acta* **2017,** *949*, 1-7.

23. Halvorson, R. A.; Vikesland, P. J., Surface-Enhanced Raman Spectroscopy (SERS) for Environmental Analyses. *Environmental Science & Technology* **2010,** *44* (20), 7749-7755.

24. Wu, D.-Y.; Li, J.-F.; Ren, B.; Tian, Z.-Q., Electrochemical surface-enhanced Raman spectroscopy of nanostructures. *Chemical Society Reviews* **2008,** *37* (5), 1025-1041.

25. Zong, C.; Chen, C.-J.; Zhang, M.; Wu, D.-Y.; Ren, B., Transient Electrochemical Surface-Enhanced Raman Spectroscopy: A Millisecond Time-Resolved Study of an Electrochemical Redox Process. *Journal of the American*

Chemical Society **2015,** *137* (36), 11768-11774.

26. Shegai, T.; Li, Z.; Dadosh, T.; Zhang, Z.; Xu, H.; Haran, G., Managing light polarization via plasmon–molecule interactions within an asymmetric metal nanoparticle trimer. *Proceedings of the National Academy of Sciences* **2008,** *105* (43), 16448-16453.

27. Tay, L.-L.; Hulse, J., Surface-enhanced Raman and optical scattering in coupled plasmonic nanoclusters. *Journal of Modern Optics* **2013,** *60* (14), 1107-1114.

28. Shiohara, A.; Wang, Y.; Liz-Marzán, L. M., Recent approaches toward creation of hot spots for SERS detection. *Journal of Photochemistry and Photobiology C: Photochemistry Reviews* **2014,** *21*, 2-25.

29. Liu, X.; Shao, Y.; Tang, Y.; Yao, K.-F., Highly Uniform and Reproducible Surface Enhanced Raman Scattering on Air-stable Metallic Glassy Nanowire Array. **2014,** *4*, 5835.

30. Lim, D.-K.; Jeon, K.-S.; Hwang, J.-H.; Kim, H.; Kwon, S.; Suh, Y. D.; Nam, J.-M., Highly uniform and reproducible surface-enhanced Raman scattering from DNA-tailorable nanoparticles with 1-nm interior gap. **2011,** *6*, 452.

31. Fan, M.; Andrade, G. F. S.; Brolo, A. G., A review on the fabrication of substrates for surface enhanced Raman spectroscopy and their applications in analytical chemistry. *Analytica Chimica Acta* **2011,** *693* (1), 7-25.

32. Tian, Z.-Q.; Ren, B.; Li, J.-F.; Yang, Z.-L., Expanding generality of surface-

enhanced Raman spectroscopy with borrowing SERS activity strategy. *Chemical Communications* **2007,** (34), 3514-3534.

33. Ding, S.-Y.; Zhang, X.-M.; Ren, B.; Tian, Z.-Q., Surface-Enhanced Raman Spectroscopy (SERS): General Introduction. In *Encyclopedia of Analytical Chemistry*, John Wiley & Sons, Ltd: 2006.

34. Cha, M. G.; Kim, H.-M.; Kang, Y.-L.; Lee, M.; Kang, H.; Kim, J.; Pham, X.-H.; Kim, T. H.; Hahm, E.; Lee, Y.-S.; Jeong, D. H.; Jun, B.-H., Thin silica shell coated Ag assembled nanostructures for expanding generality of SERS analytes. *PLOS ONE* **2017,** *12* (6), e0178651.

35. Kennedy, B. J.; Spaeth, S.; Dickey, M.; Carron, K. T., Determination of the distance dependence and experimental effects for modified SERS substrates based on self-assembled monolayers formed using alkanethiols. *J. Phys. Chem. B* **1999,** *103* (18), 3640-3646.

36. Kim, N. H.; Lee, S. J.; Kim, K., Isocyanide and biotin-derivatized Ag nanoparticles: an efficient molecular sensing mediator via surface-enhanced Raman spectroscopy. *Chemical Communications* **2003,** (6), 724-725.

37. Li, W.; Zhao, X.; Yi, Z.; Glushenkov, A. M.; Kong, L., Plasmonic substrates for surface enhanced Raman scattering. *Analytica Chimica Acta* **2017,** *984*, 19-41.

38. Mosier-Boss, P., Review of SERS Substrates for Chemical Sensing. *Nanomaterials* **2017,** *7* (6), 142.

39. Semin, D. J.; Rowlen, K. L., Influence of vapor deposition parameters on SERS active Ag film morphology and optical properties. *Analytical Chemistry* **1994,** *66* (23), 4324-4331.

40. Eickmans, J.; Otto, A.; Goldmann, A., On the annealing of "sers active" silver films: UPS and TDS of adsorbed xenon. *Surface Science* **1986,** *171* (2), 415-441.

41. Rowe, J. E.; Shank, C. V.; Zwemer, D. A.; Murray, C. A., Ultrahigh-Vacuum Studies of Enhanced Raman Scattering from Pyridine on Ag Surfaces. *Physical Review Letters* **1980,** *44* (26), 1770-1773.

42. Chao, B.-K.; Cheng, H.-H.; Nien, L.-W.; Chen, M.-J.; Nagao, T.; Li, J.-H.; Hsueh, C.-H., Anti-reflection textured structures by wet etching and island lithography for surface-enhanced Raman spectroscopy. *Applied Surface Science* **2015,** *357*, 615-621.

43. Mehrvar, L.; Sadeghipari, M.; Tavassoli, S. H.; Mohajerzadeh, S.; Fathipour, M., "Optical and Surface Enhanced Raman Scattering properties of Ag modified silicon double nanocone array". *Scientific Reports* **2017,** *7* (1), 12106.

44. Gutés, A.; Carraro, C.; Maboudian, R., Silver Dendrites from Galvanic Displacement on Commercial Aluminum Foil As an Effective SERS Substrate. *Journal of the American Chemical Society* **2010,** *132* (5), 1476-1477.

45. Jubb, A. M.; Jiao, Y.; Eres, G.; Retterer, S. T.; Gu, B., Elevated gold ellipse

nanoantenna dimers as sensitive and tunable surface enhanced Raman spectroscopy substrates. *Nanoscale* **2016,** *8* (10), 5641-5648.

46. Hatab, N. A.; Hsueh, C.-H.; Gaddis, A. L.; Retterer, S. T.; Li, J.-H.; Eres, G.; Zhang, Z.; Gu, B., Free-Standing Optical Gold Bowtie Nanoantenna with Variable Gap Size for Enhanced Raman Spectroscopy. *Nano Letters* **2010,** *10* (12), 4952-4955.

47. Kahl, M.; Voges, E.; Kostrewa, S.; Viets, C.; Hill, W., Periodically structured metallic substrates for SERS. *Sensors and Actuators B: Chemical* **1998,** *51* (1), 285-291.

48. Bryche, J.-F.; Gillibert, R.; Barbillon, G.; Gogol, P.; Moreau, J.; Lamy de la Chapelle, M.; Bartenlian, B.; Canva, M., Plasmonic Enhancement by a Continuous Gold Underlayer: Application to SERS Sensing. *Plasmonics* **2016,** *11* (2), 601-608.

49. Abu Hatab, N. A.; Oran, J. M.; Sepaniak, M. J., Surface-Enhanced Raman Spectroscopy Substrates Created via Electron Beam Lithography and Nanotransfer Printing. *ACS Nano* **2008,** *2* (2), 377-385.

50. Haynes, C. L.; Van Duyne, R. P., Nanosphere Lithography: A Versatile Nanofabrication Tool for Studies of Size-Dependent Nanoparticle Optics. *The Journal of Physical Chemistry B* **2001,** *105* (24), 5599-5611.

51. Hulteen, J. C.; Treichel, D. A.; Smith, M. T.; Duval, M. L.; Jensen, T. R.; Van Duyne, R. P., Nanosphere Lithography: Size-Tunable Silver Nanoparticle and

Surface Cluster Arrays. *The Journal of Physical Chemistry B* **1999,** *103* (19), 3854-3863.

52. Bryche, J.-F.; Tsigara, A.; Bélier, B.; de la Chapelle, M. L.; Canva, M.; Bartenlian, B.; Barbillon, G., Surface enhanced Raman scattering improvement of gold triangular nanoprisms by a gold reflective underlayer for chemical sensing. *Sensors and Actuators B: Chemical* **2016,** *228*, 31-35.

53. Mahajan, S.; Abdelsalam, M.; Suguwara, Y.; Cintra, S.; Russell, A.; Baumberg, J.; Bartlett, P., Tuning plasmons on nano-structured substrates for NIR-SERS. *Physical Chemistry Chemical Physics* **2007,** *9* (1), 104-109.

54. Päivi, S.; Nikolai, C.; Ilkka, T., The fabrication of silicon nanostructures by focused-ion-beam implantation and TMAH wet etching. *Nanotechnology* **2010,** *21* (14), 145301.

55. Freeman, R. G.; Grabar, K. C.; Allison, K. J.; Bright, R. M.; Davis, J. A.; Guthrie, A. P.; Hommer, M. B.; Jackson, M. A.; Smith, P. C.; Walter, D. G.; Natan, M. J., Self-Assembled Metal Colloid Monolayers: An Approach to SERS Substrates. *Science* **1995,** *267* (5204), 1629-1632.

56. Lee, S. J.; Baik, J. M.; Moskovits, M., Polarization-Dependent Surface-Enhanced Raman Scattering from a Silver-Nanoparticle-Decorated Single Silver Nanowire. *Nano Letters* **2008,** *8* (10), 3244-3247.

57. Fan, M.; Brolo, A. G., Self-Assembled Au Nanoparticles as Substrates for

Surface-Enhanced Vibrational Spectroscopy: Optimization and Electrochemical Stability. *ChemPhysChem* **2008,** *9* (13), 1899-1907.

58. Andrade, G. F. S.; Fan, M.; Brolo, A. G., Multilayer silver nanoparticles-modified optical fiber tip for high performance SERS remote sensing. *Biosensors and Bioelectronics* **2010,** *25* (10), 2270-2275.

59. Daniels, J. K.; Chumanov, G., Nanoparticle−Mirror Sandwich Substrates for Surface-Enhanced Raman Scattering. *The Journal of Physical Chemistry B* **2005,** *109* (38), 17936-17942.

60. Yoon, H.; Suh, J. S., Universal substrates based on Ag colloidal particles for routine surface-enhanced Raman scattering spectral measurements. *RSC Advances* **2017,** *7* (46), 28573-28579.

61. Cañamares, M. V.; Garcia-Ramos, J. V.; Gómez-Varga, J. D.; Domingo, C.; Sanchez-Cortes, S., Ag Nanoparticles Prepared by Laser Photoreduction as Substrates for in Situ Surface-Enhanced Raman Scattering Analysis of Dyes. *Langmuir* **2007,** *23* (9), 5210-5215.

62. Bjerneld, E. J.; Svedberg, F.; Käll, M., Laser-Induced Growth and Deposition of Noble-Metal Nanoparticles for Surface-Enhanced Raman Scattering. *Nano Letters* **2003,** *3* (5), 593-596.

63. Zheng, X.; Guo, D.; Shao, Y.; Jia, S.; Xu, S.; Zhao, B.; Xu, W.; Corredor, C.; Lombardi, J. R., Photochemical Modification of an Optical Fiber Tip with a

Silver Nanoparticle Film: A SERS Chemical Sensor. *Langmuir* **2008,** *24* (8), 4394-4398.

64. Taylor, R. W.; Esteban, R.; Mahajan, S.; Aizpurua, J.; Baumberg, J. J., Optimizing SERS from Gold Nanoparticle Clusters: Addressing the Near Field by an Embedded Chain Plasmon Model. *The Journal of Physical Chemistry C* **2016,** *120* (19), 10512-10522.

65. Su, Q.; Ma, X.; Dong, J.; Jiang, C.; Qian, W., A Reproducible SERS Substrate Based on Electrostatically Assisted APTES-Functionalized Surface-Assembly of Gold Nanostars. *ACS Applied Materials & Interfaces* **2011,** *3* (6), 1873-1879.

66. Shin, H. S.; Yang, H. J.; Jung, Y. M.; Kim, S. B., Direct patterning of silver colloids by microcontact printing: possibility as SERS substrate array. *Vibrational Spectroscopy* **2002,** *29* (1), 79-82.

67. Cho, W. J.; Kim, Y.; Kim, J. K., Ultrahigh-Density Array of Silver Nanoclusters for SERS Substrate with High Sensitivity and Excellent Reproducibility. *ACS Nano* **2012,** *6* (1), 249-255.

68. Nery, E. W.; Kubota, L. T., Sensing approaches on paper-based devices: a review. *Analytical and Bioanalytical Chemistry* **2013,** *405* (24), 7573-7595.

69. Cabalín, L. M.; Laserna, J. J., Fast spatially resolved surface-enhanced Raman spectrometry on a silver coated filter paper using charge-coupled device

detection. *Analytica Chimica Acta* **1995,** *310* (2), 337-345.

70. Lee, A. S. L.; Li, Y.-S., Surface-enhanced Raman spectra using silver-coated paper substrates. *Journal of Raman Spectroscopy* **1994,** *25* (3), 209-214.

71. Lee, C. H.; Hankus, M. E.; Tian, L.; Pellegrino, P. M.; Singamaneni, S., Highly Sensitive Surface Enhanced Raman Scattering Substrates Based on Filter Paper Loaded with Plasmonic Nanostructures. *Analytical Chemistry* **2011,** *83* (23), 8953-8958.

72. Lee, C. H.; Tian, L.; Singamaneni, S., Paper-Based SERS Swab for Rapid Trace Detection on Real-World Surfaces. *ACS Applied Materials & Interfaces* **2010,** *2* (12), 3429-3435.

73. Yu, W. W.; White, I. M., A simple filter-based approach to surface enhanced Raman spectroscopy for trace chemical detection. *Analyst* **2012,** *137* (5), 1168-1173.

74. Rajapandiyan, P.; Yang, J., Photochemical method for decoration of silver nanoparticles on filter paper substrate for SERS application. *Journal of Raman Spectroscopy* **2014,** *45* (7), 574-580.

75. Cheng, M.-L.; Tsai, B.-C.; Yang, J., Silver nanoparticle-treated filter paper as a highly sensitive surface-enhanced Raman scattering (SERS) substrate for detection of tyrosine in aqueous solution. *Analytica Chimica Acta* **2011,** *708* (1), 89-96.

76. Li, Y.; Zhang, K.; Zhao, J.; Ji, J.; Ji, C.; Liu, B., A three-dimensional silver

nanoparticles decorated plasmonic paper strip for SERS detection of low-abundance molecules. *Talanta* **2016,** *147*, 493-500.

77. Yu, C.-C.; Chou, S.-Y.; Tseng, Y.-C.; Tseng, S.-C.; Yen, Y.-T.; Chen, H.-L., Single-shot laser treatment provides quasi-three-dimensional paper-based substrates for SERS with attomolar sensitivity. *Nanoscale* **2015,** *7* (5), 1667-1677.

78. Qu, L.-L.; Li, D.-W.; Xue, J.-Q.; Zhai, W.-L.; Fossey, J. S.; Long, Y.-T., Batch fabrication of disposable screen printed SERS arrays. *Lab on a Chip* **2012,** *12* (5), 876-881.

79. Qu, L.-L.; Song, Q.-X.; Li, Y.-T.; Peng, M.-P.; Li, D.-W.; Chen, L.-X.; Fossey, J. S.; Long, Y.-T., Fabrication of bimetallic microfluidic surface-enhanced Raman scattering sensors on paper by screen printing. *Analytica Chimica Acta* **2013,** *792*, 86-92.

80. Liu, Q.; Wang, J.; Wang, B.; Li, Z.; Huang, H.; Li, C.; Yu, X.; Chu, P. K., Paper-based plasmonic platform for sensitive, noninvasive, and rapid cancer screening. *Biosensors and Bioelectronics* **2014,** *54*, 128-134.

81. Kim, W.; Kim, Y.-H.; Park, H.-K.; Choi, S., Facile Fabrication of a Silver Nanoparticle Immersed, Surface-Enhanced Raman Scattering Imposed Paper Platform through Successive Ionic Layer Absorption and Reaction for On-Site Bioassays. *ACS Applied Materials & Interfaces* **2015,** *7* (50), 27910-27917.

82. Huang, Z.; Cao, G.; Sun, Y.; Du, S.; Li, Y.; Feng, S.; Lin, J.; Lei, J.,

Evaluation and Optimization of Paper-Based SERS Substrate for Potential Label-Free Raman Analysis of Seminal Plasma. *Journal of Nanomaterials* **2017,** *2017*, 8.

83. Saha, A.; Jana, N. R., Paper-Based Microfluidic Approach for Surface-Enhanced Raman Spectroscopy and Highly Reproducible Detection of Proteins beyond Picomolar Concentration. *ACS Applied Materials & Interfaces* **2015,** *7* (1), 996-1003.

84. Hwang, J.; Lee, S.; Choo, J., Application of a SERS-based lateral flow immunoassay strip for the rapid and sensitive detection of staphylococcal enterotoxin B. *Nanoscale* **2016,** *8* (22), 11418-11425.

85. Wang, X.; Choi, N.; Cheng, Z.; Ko, J.; Chen, L.; Choo, J., Simultaneous Detection of Dual Nucleic Acids Using a SERS-Based Lateral Flow Assay Biosensor. *Analytical Chemistry* **2017,** *89* (2), 1163-1169.

86. Wang, P.; Zhou, Y.; Wen, Y.; Wang, F.; Yang, H., In situ polydopamine-assisted deposition of silver nanoparticles on a two dimensional support as an inexpensive and highly efficient SERS substrate. *RSC Advances* **2015,** *5* (46), 36368-36373.

87. Zhang, K.; Zhao, J.; Xu, H.; Li, Y.; Ji, J.; Liu, B., Multifunctional Paper Strip Based on Self-Assembled Interfacial Plasmonic Nanoparticle Arrays for Sensitive SERS Detection. *ACS Applied Materials & Interfaces* **2015,** *7* (30), 16767-16774.

88. Creighton, J. A.; Blatchford, C. G.; Albrecht, M. G., Plasma resonance enhancement of Raman scattering by pyridine adsorbed on silver or gold sol particles of size comparable to the excitation wavelength. *Journal of the Chemical Society, Faraday Transactions 2: Molecular and Chemical Physics* **1979,** *75* (0), 790-798.

89. Draine, B. T.; Flatau, P. J., Discrete-Dipole Approximation For Scattering Calculations. *J. Opt. Soc. Am. A* **1994,** *11* (4), 1491-1499.

90. Palik, E. D., *Handbook of Optical Constants of Solids*. Academic Press: 1998.

91. Currie, L. A., Limits for qualitative detection and quantitative determination. Application to radiochemistry. *Analytical Chemistry* **1968,** *40* (3), 586-593.

92. Haslach, H. W., The Moisture and Rate-Dependent Mechanical Properties of Paper: A Review. *Mechanics of Time-Dependent Materials* **2000,** *4* (3), 169-210.

93. Shimada, T.; Imura, K.; Hossain, M. K.; Okamoto, H.; Kitajima, M., Near-Field Study on Correlation of Localized Electric Field and Nanostructures in Monolayer Assembly of Gold Nanoparticles. *The Journal of Physical Chemistry C* **2008,** *112* (11), 4033-4035.

94. Hasi, W.-L.-J.; Lin, X.; Lou, X.-T.; Lin, S.; Yang, F.; Lin, D.-Y.; Lu, Z.-W., Chloride ion-assisted self-assembly of silver nanoparticles on filter paper as SERS substrate. *Applied Physics A* **2015,** *118* (3), 799-807.

95. Hasi, W.-L.-J.; Lin, S.; Lin, X.; Lou, X.-T.; Yang, F.; Lin, D.-Y.; Lu, Z.-W., Rapid fabrication of self-assembled interfacial film decorated filter paper as an excellent surface-enhanced Raman scattering substrate. *Analytical Methods* **2014,** *6* (24), 9547-9553.

96. Jayawardhana, S.; Rosa, L.; Buividas, R.; Stoddart, P. R.; Juodkazis, S., Light enhancement in surface-enhanced Raman scattering at oblique incidence. *Photonic Sensors* **2012,** *2* (3), 283-288.

97. Tang, M.; Wang, X.; Xianguang, F.; Li, W.; Xu, Y.; Que, J.; He, J.; Zuo, Y., High sensitivity and resolution integrated optical system for portable Raman spectrometer. *Appl. Opt.* **2016,** *55* (26), 7195-7203.

98. Chrimes, A. F.; Khoshmanesh, K.; Stoddart, P. R.; Mitchell, A.; Kalantar-zadeh, K., Microfluidics and Raman microscopy: current applications and future challenges. *Chemical Society Reviews* **2013,** *42* (13), 5880-5906.

99. Oh, K.; Lee, J.-H.; Im, W.; Rajabi Abhari, A.; Lee, H. L., Role of Cellulose Nanofibrils in Structure Formation of Pigment Coating Layers. *Industrial & Engineering Chemistry Research* **2017,** *56* (34), 9569-9577.

100. Sun, Z.; Du, J.; Yan, L.; Chen, S.; Yang, Z.; Jing, C., Multifunctional Fe3O4@SiO2–Au Satellite Structured SERS Probe for Charge Selective Detection of Food Dyes. *ACS Applied Materials & Interfaces* **2016,** *8* (5), 3056-3062.

101. Joshi, G. K.; Smith, K. A.; Johnson, M. A.; Sardar, R., Temperature-

Controlled Reversible Localized Surface Plasmon Resonance Response of Polymer-Functionalized Gold Nanoprisms in the Solid State. *The Journal of Physical Chemistry C* **2013,** *117* (49), 26228-26237.

102. Mock, J. J.; Smith, D. R.; Schultz, S., Local Refractive Index Dependence of Plasmon Resonance Spectra from Individual Nanoparticles. *Nano Letters* **2003,** *3* (4), 485-491.

요 약

(국문 초록)

미량의 농약 검출을 위한 효율적인 방법 중에 하나로 각광받는 필터 페이퍼 기반의 표면 증강 라만 산란 (SERS) 센서는 지난 십수년간 연구되어 왔다. 그러나 필터 페이퍼의 친수성 성질에 의해 용액들은 종이 표면에 고정되지 않고 빠르게 종이 내부로 흡수되게 될 뿐만 아니라 종이를 구성하는 셀룰로오스 섬유의 구조적, 크기적 다양성에 의해 많은 수의 공극과 높은 종이 표면 단차를 보여주고 있다. 이러한 종이의 특성으로 인해 낮은 종이 기반의 SERS 센서의 감도와 재현성이 나타났다. 또한 분자와 금속 사이의 결합력 차이에 의해 일부의 분자만 검출이 가능하며 다양한 분자를 검출할 수 있는 범용적 센서로는 사용이 어려웠다.

본 연구에서는 이러한 기존의 종이의 특성에 의해 발생하는 단점을 극복하고 고감도, 고재현성의 SERS 신호를 내는 필터 페이퍼 기반 SERS 센서를 개발하였다. 우선 필터 페이퍼 기반의 SERS 센서의 감도를 높이기 위하여 알킬케텐다이머를 (AKD) 종이에 처리하여 필터 페이퍼의 친수성 성질을 소수성으로 개질하였다. 또한 소수성 처리된 필터 페이퍼 표면에 셀룰로오스 나노섬유를 (CNF) 도입하여 종이 표면의 단차 및 공극을 줄여 필터 페이퍼 기반 SERS 센서의 표면의 균일성을 증가시켰다. 이를 기반으로 필터 페이퍼 기반의 SERS 센서의 재현성을 높이고자 하였다. 마지막으로 기존에 검출이 어려웠던 극성 유기 분자의 검출이 가능한 필터 페이퍼 기반의 SERS 센서를 개발하기 위해 서로 다른 전하를 가지는 나노입자를 도입하여 전하 선택적 검출이 가능한 필터 페이퍼 기반의 SERS 센서를 제작하였고 이를 통해 SERS 기반의 분자 검출의 보편성을

확장하고자 하였다. 그렇기에 본 연구는 크게 소수성 처리를 통한 고감도 필터 페이퍼 기반 SERS 센서 제작, 셀룰로오스 나노섬유의 도입을 이용한 고재현성을 나타내는 필터 페이퍼 기반 SERS 센서 제작, 마지막으로 극성 유기 분자 검출을 위한 전하 선택적 검출을 도입한 필터 페이퍼 기반 SERS 센서를 제작 및 적용 이렇게 세 파트로 구성되어 있다.

챕터 1에서는 소수성으로 개질된 필터 페이퍼의 개발에 대해서 다루고 있다. 기존의 종이 기반의 SERS 센서는 친수성의 성질로 인해 용액이 종이 내부로 빠르게 흡수되어 종이 표면에 나노입자가 거의 존재하지 않았으며 또한 분석 물질이 나노입자와 결합하기에 시간이 충분치 않아 낮은 SERS 신호 민감도와 재현성을 나타냈다. 이를 개선하기 위해 종이에 AKD 처리를 통해 소수성 성질을 나타내도록 하였다. 소수성 개질을 통해 종이 표면에서 수용액의 접촉각과 유지 시간이 증가하였으며, 증가된 접촉각으로 인해 용액의 접촉 면적이 감소하였다. 이로 인해 종이 표면에 은 나노입자 (AgNP) 의 밀도가 증가하게 되어 수많은 SERS hot-spot 을 형성하였고, 이로 인해 SERS 신호의 급격하게 증가하였다. 또한 AgNP 용액의 농도를 조절하여 필터 페이퍼 위의 AgNP 분포를 조절하였으며, 이를 통해 SERS 신호의 민감도와 재현성을 최적화 하였다. 이를 통해 개발한 종이 기반의 SERS 센서는 6.19%의 SERS 신호의 표준 편차를 나타냈으며 thiram 과 ferbam 이 각각 0.461 nM 과 0.491 nM 의 검출 한계를 나타냄을 확인하였다. 이 결과를 통해 종이의 소수성 처리를 통해 저렴하고 쉬운 방법으로 미량의 농약을 높은 재현성으로 검출 할 수 있는 필터 페이퍼 기반의 SERS 센서를 개발 할 수 있음을 확인하였다.

챕터 2에서는 CNF 코팅 도입을 통해 종이 표면의 단차 및 공극을 줄여 종이 기반의 SERS 센서의 신호 재현성을 증가시키는 것에 대해 다루고 있다. 많은 수의 공극과 높은 표면 단차에 의해 종이 표면은 불균일한

특성을 나타내며 이로 인해 기존의 종이 기반의 SERS 센서는 낮은 SERS 신호 재현성을 나타내고 있다. 이를 극복하기 위해 CNF 코팅을 도입하여 종이 표면의 공극을 채우고 표면 단차를 줄이고자 하였다. 두 번의 CNF 코팅의 도입에 따라 필터 페이퍼의 표면에서의 AgNP 커버리지가 87% 에서 95% 까지 증가됨을 확인하였으며, CNF 코팅 도입에 따른 종이 표면의 표면 단차 감소 및 공극의 수 감소로 인해 AgNP 가 균일하게 도입됨을 FE-SEM 이미지 분석을 통해 확인할 수 있었다. 이를 통해 두 번의 CNF 코팅을 필터 페이퍼에 도입함에 따라 SERS 신호의 상대 표준 편차는 28%에서 9%로 감소하였으며 4-ATP 의 검출 한계는 3.782 nM 에서 0.426 nM 로 감소하는 것을 확인하였다. CNF 코팅 도입에 따른 표면 균일성 증가는 SERS 신호 재현성 뿐만 아니라 신호 민감도까지 증가시킴을 확인하였고 이는 종이 기반의 SERS 센서의 신호 재현성의 증가에 기본 연구가 될 수 있음을 확인하였다.

마지막으로 챕터 3 에서는 극성 유기 분자를 검출 할 수 있는 전하 선택적 종이 기반의 SERS 센서 개발에 대해서 다루고 있다. 분자에 있는 작용기에 따라 분자와 금속은 서로 다른 친화도를 나타내며, 이로 인해 기존의 종이 기반의 SERS 센서는 특정한 분자만 검출 가능하였다. 이를 극복하고 SERS 기반의 분자 검출의 보편성을 확대시키기 위해 본 연구에서는 전하 선택적 검출이 가능한 종이 기반의 SERS 센서를 제작하였다. 이를 위해 서로 다른 전하를 가지는 AgNP를 필터 페이퍼에 도입하여 전하 선택적 종이 기반의 SERS 센서를 개발하였다. 기존의 AgNP은 시트르산 이온에 의해 음전하를 나타내며, 이러한 AgNP 표면에 양전하를 띄는 고분자인 poly(allyldimethylammonium chloride) (PDDA)을 도입한 AgNP@PDDA를 개발하여 양전하를 나타내는 나노 입자를 개발하였다. 서로 다른 전하를 나타내는 AgNP와 AgNP@PDDA를 종이 표면에 도입

하여 전하 선택적 검출이 가능한 종이 기반의 SERS 센서를 개발하였다. AgNP에 PDDA 고분자가 도입됨을 UV/Vis 스펙트럼, 제타 전위 변화 및 고해상도 투과 전자 현미경을 이미지 변화를 통해 확인하였다. 제작한 센서의 전하 선택적 검출의 적용 가능성을 확인하기 위해 전하를 띄는 라만 염료를 각각의 센서에 적용하였으며 AgNP 가 처리된 센서에서는 양전하를 띈 라만 염료가, AgNP@PDDA 가 처리된 센서에서는 음전하를 띈 라만 염료가 검출됨을 확인하였고, 이는 나노 입자와 전하를 띄는 분자 사이에 작용하는 정전기적 인력에 의해서 나타남을 확인하였다. 이를 통해 개발된 전하 선택적 종이 기반의 SERS 센서의 전하 선택적 분자 검출 적용 가능성을 확인하였고, 극성 유기 분자의 검출 확인을 위해 아닐린과 벤조산 유도체를 도입하였다. 각각의 극성 유기 분자는 AgNP 및 AgNP@PDDA 센서에서 분리 검출됨을 확인되었으며, 아닐린과 벤조산이 수십 마이크로 몰 농도의 수준까지 검출됨을 확인하였다. 또한 10% 이하의 상대 표준 편차를 나타냄을 확인하였으며 이를 통해 개발한 전하 선택적 종이 기반의 SERS 센서를 이용하여 기존의 검출이 어려웠던 분자를 고감도, 고재현성 검출이 가능함을 확인하였다. 본 연구에서 제시한 종이 기반의 SERS 센서 개발은 종이 기반의 SERS 센서의 기초 연구로서 다른 연구의 길잡이가 될 수 있을 것이라 생각한다.

주요어 : 표면 증강 라만 산란, 알킬케텐다이머, 필터 페이퍼, 종이 기반 표면 증강 라만 산란 센서, 소수성 개질, 감도, 재현성, 셀룰로오스 나노섬유, 전하 선택적 표면 증강 라만 산란 검출

학 번 : 2012-30411